RF HEATING OF LASER-INDUCED GRAPHITE (LIG) ON POLYMER SURFACES

A Thesis

by

JOSEPH CARR GERRINGER

Submitted to the Office of Graduate and Professional Studies of
Texas A&M University
in partial fulfillment of the requirements for the degree of

MASTER OF SCIENCE

Chair of Committee,	Micah J. Green
Committee Members,	Svetlana Sukhishvili
	Mohammad Naraghi
Head of Department,	Ibrahim Karaman

August 2019

Major Subject: Materials Science and Engineering

Copyright 2019 Joseph Gerringer

ABSTRACT

In this report, we investigate laser-induced graphite (LIG) structures formed in polymeric substrates in order to quantify LIG heating response to radio frequency (RF) fields. Graphitic structures were produced from various polymeric substrates via laser irradiation of the polymer surface. We find that RF responsive, graphitic structures may be produced from polyimide (PI), polyether imide (PEI), polyether sulfone (PESU), polyether ether ketone (PEEK), and polycarbonate (PC) using a conventional laser cutting machine. The graphitic structures are also conductive in addition to being RF responsive. Exposure of LIG to RF fields resulted in the rapid heating of LIG with heating rates up to 126 °C/s. This heating response may be used in advanced manufacturing as a means to rapidly weld polymer-polymer interfaces, as will be demonstrated in this report. This technique uses RF fields to induce localized heating in contrast to uniform heating from external sources such as ovens or furnaces. Finally, we aim to determine how LIG-polymer composites may function in an industrial setting, with particular application to additive manufacturing and functional coatings. One novel application of these findings is the potential use of LIG-polymer heating elements on thermoplastic filaments for welding 3D-printed filament traces together and improving the isotropic strength of 3D-printed structures. First, we review the necessary background information on LIG formation, thermoplastic joining, and nanomaterial heating in response to electromagnetic fields. We then describe the laser etching procedure used to produce graphitic structures from neat polymer substrates. The method and experimental setup required to generate RF

fields and subsequent RF field heating are also addressed. The proposed work would enable entirely new techniques for polymer processing, where the RF responsive filler is generated *in situ*.

ACKNOWLEDGEMENTS

I would like to thank my committee chair, Dr. Green, and my committee members, Dr. Sukhishvili and Dr. Naraghi, for their guidance and support throughout the course of this research. I would like to extend special thanks to Dr. Green for providing continued direction and assistance throughout the duration of my time as a graduate student at Texas A&M. Dr. Green has made my graduate school experience both enjoyable and fulfilling. I wish more professors possessed the care and enthusiasm that Dr. Green has for his students and his work. Any problems that I may have had, related to work or otherwise, I knew that I could rely on Dr. Green for help.

Thanks also go to my friends and colleagues and the Materials Science and Engineering department faculty and staff for making my time at Texas A&M University a great experience. I would especially like to thank Jules Henry for her guidance during my years as an undergraduate and graduate student.

Finally, thanks to my mother and father for their encouragement and guidance. I would not have been able to make it thus far without their support.

CONTRIBUTORS AND FUNDING SOURCES

Contributors

This work was supervised by a thesis committee consisting of Professor Micah Green (advisor) of the Department of Chemical Engineering and Professor(s) Mohammad Naraghi of the Department of Aerospace Engineering and Svetlana Sukhishvili of the Department of Materials Science and Engineering.

I would also like to thank Dr. Blake Teipel, CEO of Essentium, and Dr. Brandon Sweeney, head of R&D for materials at Essentium, for their guidance and support throughout the duration of my graduate studies at Texas A&M. I knew that I could rely on Dr. Sweeney and Dr. Teipel for consultation (as it relates to 3D printing), as well as providing many of the raw materials used in this study.

Much of my RF heating related training was administered by Nutan Patil, a chemical engineering Ph.D. candidate in Dr. Green's group. Nutan was especially helpful in the initial stages of this study, as I was becoming familiar with the equipment in the Green lab. I would also like to extend thanks to Aaron Moran, an undergraduate student conducting research under Dr. Green. Aaron has assisted me in the RF characterization and preliminary additive manufacturing results listed in Chapter 3. Thanks is also extended to all current and previous Green lab members for their input during group meetings.

Raman spectroscopy data was provided by Cristen Corry, a Ph.D. candidate in the Department of Chemistry at Texas A&M. Special thanks to Professor Matthew Sheldon

in the Department of Chemistry for allowing Cristen and I to work together to obtain this data.

All other work conducted for the thesis (or) dissertation was completed by the student independently.

Funding Sources

Graduate study was supported by a research grant from the U.S. National Science Foundation (CMMI-1561988). Its contents are solely the responsibility of the authors and do not necessarily represent the official views of the Foundation.

NOMENCLATURE

LIG	Laser-induced graphite
PC	Polycarbonate
PEEK	Polyether ether ketone
PEI	Polyether imide (Ultem)
PESU	Polyether sulfone
PI	Polyimide (Kapton)
RF	Radio frequency

TABLE OF CONTENTS

Page

ABSTRACT ii

ACKNOWLEDGEMENTS iv

CONTRIBUTORS AND FUNDING SOURCES v

NOMENCLATURE vii

TABLE OF CONTENTS viii

LIST OF FIGURES x

LIST OF TABLES xiii

1. INTRODUCTION 1

1.1. Laser-Polymer Interactions 2
1.2. Polymer Bonding 5
1.3. Nanomaterial Response to RF Fields 6

2. EXPERIMENTAL METHODS 10

2.1. LIG Production on Polymer Substrates 10
2.2. Characterizing LIG Structures 12
2.3. Measuring RF Response 12
2.4. Welding Preparation and Mechanical Characterization 15
2.5. Printing with LIG Filament 18

3. RESULTS 20

3.1. LIG Formation and Characterization 20
3.2. LIG@Polymer RF Heating 27
3.3. Rapid Welding of Polymer Surfaces 34
3.4. Additive Manufacturing 39

4. CONCLUSIONS AND FUTURE WORKS 41

REFERENCES 43

APPENDIX A 49

Page

APPENDIX B 52

LIST OF FIGURES

Page

Figure 1-1. (A) Laser irradiation can graphitize certain polymer surfaces. (B) We aim to prove that this graphitic material will heat in response to RF fields, allowing for polymeric surfaces to be welded together without the need for an external heating source. (C) A cross-section of polymer interface shows the mechanism behind this hypothesis: The dark LIG structure heats upon exposure to RF fields, which in turn allows for polymer chains to diffuse across the interface and form a weld. 1

Figure 1-2. Geometry illustrations (top) and corresponding FLIR thermal image (bottom) showing three RF electric field applicator configurations: (A) direct contact, (B) parallel plate, and (C) interdigitated fringing field. These three applicators are applied to three samples: (D) 1.0 wt.% MWCNT in PLA at 315 W, 100 MHz, 4 seconds; (E) 7.5 wt.% MWCNT in PLA at 100 W, 100 MHz, 6 seconds; (F) 1.0 wt.% MWCNT in PLA at 315 W, 50 MHz, 1 second. [Figure and caption reprinted with permission from Green *et al.* Radio frequency heating of carbon nanotube composite materials. *ACS Applied Materials & Interfaces* 2018, *10*, 27252-27259. Copyright 2018 American Chemical Society.] 8

Figure 2-1. Schematic of the main areas of research, which include: sample preparation, sample characterization, determining RF heating response, sample welding, and 3D printing. 10

Figure 2-2. (A) Signal generator and amplifier used to produce RF fields. (B) Typical experimental setup for testing the RF field response of each LIG@polymer system. The setup shown here also displays a typical LIG@Kapton sample used for quantifying RF heating. 13

Figure 2-3. (A) To create lap-shear test samples, we use two polymer coupons, each is patterned with LIG stripes using the laser. (B) The coupons are placed in contact with each other prior to being placed atop a capacitor with a fringing RF field. (C) The fringing field will induce heating in LIG and polymer bonding. This allows for rapid, non-contact, non-oven welding. 15

Figure 2-4. (A) PEI film that has been patterned with LIG stripes (5% laser power, 10% etch speed, 1000 PPI). (B) The weld sample is assembled after determining that the bottom coupon and the reference are heating at the same rate. (C) The welded sample has a weld area that is localized between the copper strips and spans over the length of the sample. 16

Page

Figure 2-5. (A) FLIR image that was captured after 20 s of RF exposure (103 MHz, 2.0 W). An image showing the sample and reference orientation with respect to the RF applicator is also included (both prepared with 5% laser power, 10% etch speed, 1000 PPI). (B/C) Plots showing the maximum temperature of the weld sample (B) and reference (C) recorded by the FLIR camera over time. In these plots, time "0" corresponds to the moment when the RF field was engaged. 17

Figure 2-6. A prototype LIG@PESU printing filament developed at TAMU (5% laser power, 10% etch speed, 1000 PPI). Filament diameter is 1.75 mm, typical for material extrusion 3D printers. 19

Figure 3-1. A 76.2 mm x 76.2 mm sample of Kapton that has been etched by a CO_2 laser (30% laser power, 50% etch speed, 1000 PPI). The pattern displayed was designed prior to lasing using AutoCAD. 22

Figure 3-2. Raman spectrum of LIG@Kapton (excitation wavelength = 532 nm). We observe three distinct peaks: D (1352 cm^{-1}), G (1580 cm^{-1}), and 2D (2678 cm^{-1})..... 23

Figure 3-3. Optical microscopy images taken of (A) LIG@PEI (scale bar=100 µm) and (B) LIG@PESU (scale bar=200 µm) stripes. The dark regions are LIG, while the light regions are areas of the parent polymer that were not converted to LIG during the laser etching process. Both samples were prepared with 5% laser power, 10% etch speed, and 1000 PPI. 24

Figure 3-4. Optical microscopy images (scale bar=100 µm) of a single laser pass on PEI produced with 1000 PPI (A) and 300 PPI (B). 5% laser power and 10% etch speed were used in both cases. 25

Figure 3-5. Optical microscopy images (scale bar=100 µm) taken of a single LIG@Kapton sample (30% laser power, 50% etch speed, 1000 PPI). (A) The unaltered sample (after laser treatment) clearly shows the pathway of the laser and resulting porous LIG structure. (B) After solvent-treating the LIG regions in (A), porosity is reduced and LIG connectivity increases. 26

Figure 3-6. (A) Temperature distribution across a LIG@Kapton sample during RF field exposure (30% laser power, 50% etch speed, 1000 PPI). (B) Heating response of the sample in (A) as a function of the frequency of the applied RF field. The power of the RF field in both cases was 10 W. 28

Page

Figure 3-7. Plot showing steady state temperature as a function of RF power in LIG@Kapton samples (30% laser power, 50% etch speed, 1000 PPI) during constant RF exposure (fixed frequency of 105 MHz). 30

Figure 3-8. Plot displaying maximum temperature at 5 seconds of RF exposure (10 W of Power, 103 MHz) as a function of laser PPI on LIG@PEI (5% laser power, 10% etch speed, 1000 PPI). 31

Figure 3-9. Plot displaying temperature over 30 seconds of constant RF heating (10 W of Power, 103 MHz) for samples prepared with 5% (blue), 7% (red), and 10% (green) laser power (10% etch speed and 1000 PPI used in all cases). Time "0" corresponds to the moment when the RF field was engaged. 33

Figure 3-10. Thermal image of unaltered (A) and solvent-treated (B) LIG@Kapton during RF exposure (30% laser power, 50% etch speed, 1000 PPI). Temperature profiles show the maximum temperature reached in 30 seconds of RF heating (10 W of Power, 105 MHz). 34

Figure 3-11. (A) A set of LIG@PEI welded samples. This image shows that weld area is consistent, suggesting that this RF welding process is reproducible. (B-D) Images of a single LIG@PEI sample, showing top (B), bottom (C), and side (D) views. 37

Figure 3-12. Weld strength as a function of RF exposure time plotted on a logarithmic scale. The red dotted-line represents the trendline for this data set. 38

Figure 3-13. (A/B) Optical microscopy images (scale bar=200 μm) of LIG@PEI stripes after welding and lap shear testing. The structural integrity of LIG stripes is maintained throughout the welding process. 39

Figure 3-14. (A) Thermal image of LIG@PI filament during RF field exposure (30% laser power, 50% etch speed, 1000 PPI). (B) Heating rates up to 34.5 °C/s allow for rapid heating of LIG@PI filament pre and post print. 40

LIST OF TABLES

Page

Table 3-1. Optimized laser parameters used to prepare each LIG@polymer system for quantifying RF heating rates. 21

Table 3-2. Maximum heating rates for each LIG@polymer system observed during RF frequency sweeps at a constant power of 10W. The frequencies which induced maximum heating rates for all systems are also shown. The laser parameters used to prepare these samples are listed in Table 3-1. 29

Table 3-3. Average weld strength of welded LIG@PEI coupons at various RF exposure times. Samples were prepared as depicted in Figure 2-4. 36

1. INTRODUCTION

In this report, we test two key hypotheses: (i) Laser-induced graphite (LIG) structures formed in polymeric substrates will rapidly heat in response to RF fields, such that (ii) this heating response may be used in advanced manufacturing as a means to rapidly weld polymer-polymer interfaces. As shown in Figure 1-1, we produce graphitic material on the polymer surface via laser irradiation. The localized heat generated during RF field exposure promotes polymer diffusion and creates a weld between two polymer surfaces. First, we review previous work dealing with laser-polymer interactions. The topics of welding polymer interfaces and other RF responsive nanomaterials, such as carbon nanotubes (CNTs),[1,2] are also addressed.

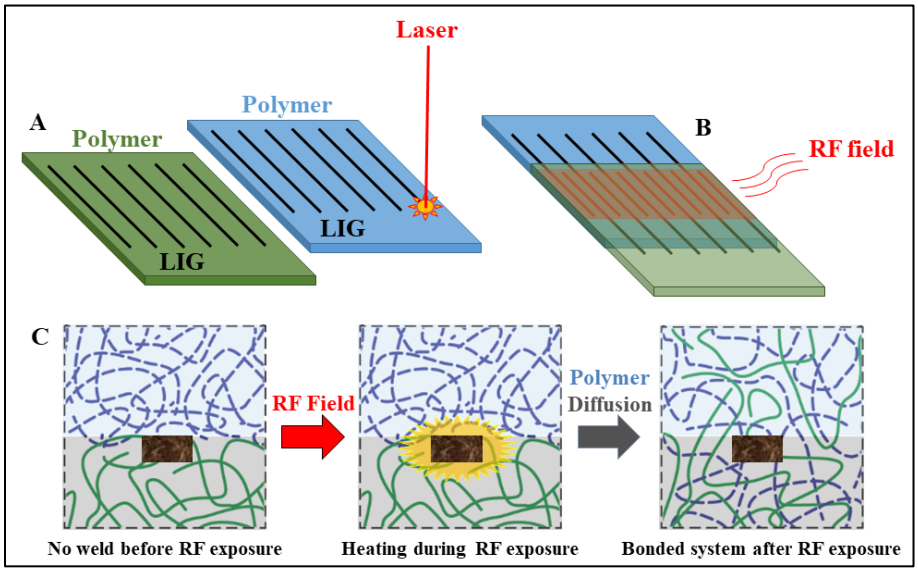

Figure 1-1. (A) Laser irradiation can graphitize certain polymer surfaces. (B) We aim to prove that this graphitic material will heat in response to RF fields, allowing for polymeric surfaces to be welded together without the need for an external heating source. (C) A cross-section of polymer interface shows the mechanism behind this hypothesis: The dark LIG structure heats upon exposure to RF fields, which in turn allows for polymer chains to diffuse across the interface and form a weld.

1.1. Laser-Polymer Interactions

Laser irradiation is a promising technique for converting polymers into carbonaceous, electrically conductive structures. The process of producing conductive material from organic precursors using lasers was first reported in the late 1980s for the etching of polyimide (PI) by an Argon laser (488 nm).[3] Prior to this report, the production of conductive carbonaceous material from polymers was typically done through destructive methods such as pyrolysis.[4] The laser-produced material was generally classified as glassy (non-graphitic), crystalline, non-porous carbon, and the material properties (crystallinity, elemental composition, electrical conductivity) were influenced by the type of laser.[5-10] For example, multiple continuous-wave UV lasers (wavelengths ranging from 275-373 nm or 350-380 nm) have been used on PI.[5,6] A variety of pulsed excimer lasers have also been used for this etching process, but each resulted in the formation of glassy carbon with polycrystalline domains.[7-10] There has been relatively little mention of formation of few-layer graphitic structures in these studies.

However, a new method has recently been developed in this context by the Tour group at Rice University.[11] Their method produces graphitic structures from polymer precursors through a simple laser etching process.[11] The morphology of these porous graphitic structures from polymer samples is quite different from the glassy carbon results described above. This technique developed by Tour *et al*. has attracted significant attention because of its ability to produce graphitic structures from a wide range of precursor materials. (Note that this material can be considered as “graphene”, depending upon one’s definitions; the Rice group does use the term “graphene,” but they do note that the term is

somewhat controversial in this context. We de-emphasize the "graphene" vs. "graphite" debate in this report since the key issue here is the RF heating properties that are important in the research plan below, not the nanomaterial terminology. Therefore, we refer to this material as laser-induced graphite (LIG) for the purposes of this study) Note that this production method is radically different than historic top-down graphene production (where graphene is exfoliated from bulk graphite) or bottom-up graphene production (where graphene is grown using chemical vapor deposition from small-molecule reactants). The conversion process involves exposing a neat polymer substrate to a CO_2 laser with a preset power and frequency. Tour *et al*. reported that the exposure time (which is controlled by the laser etching speed), power, and frequency of the laser must be tailored to the chemical structure of the chosen precursor material in order to successfully form LIG.[11,12] Only the areas of the substrate exposed to the laser will be converted into LIG, such that this laser etching process is spatially controllable.[13]

A proposed mechanism for this process is that the precursor material (Kapton or other aromatic polymers) undergoes a photothermal conversion process during lasing, with a transition from sp^3 to sp^2 hybridization.[11] Lasing causes a high degree of lattice vibrations to propagate through the precursor material,[11,14] and the energy associated with these vibrations leads to the generation of localized heat within the precursor material, sufficient to break C-N, C-O, and C=O bonds (in the case of Kapton).[14] More recent work suggests that there may be an amorphous carbon intermediate state before final conversion to a graphitic structure, meaning that multiple lases may be needed to produce LIG.[13]

However, this transition from amorphous carbon to LIG may not occur if the incorrect laser is chosen,[5-7] or if the threshold energy required to produce LIG is not met.[11-13]

As stated above, LIG formation is dependent upon the power level and speed of the laser, both of which control how much energy is exposed to the sample during laser contact. Laser power determines the amount of energy that the sample is exposed to per second of lasing at a single laser contact point, and directly affects the depth at which graphitic material is formed at each contact point. Conversely, the speed of the laser controls the amount of time that the laser is in engaged with the sample at any given contact point, with lower speeds corresponding to longer contact times (and thus larger amounts of energy) while etching a sample. Tour suggests that multiple combinations of power level and speed may be used to form LIG on Kapton, as long as the threshold energy required to produce LIG is reached.[11] Given that a pulsing laser was used in this study, the number of laser contacts per inch of material (formally referred to as points per inch or PPI) can also affect LIG production. PPI controls how frequently the laser contacts the sample by dialing in the spacing between laser contact points. This means that the areal density of contact points, and the depth of material formed at each of those points, can be controlled. Note also that the laser path may be spatially patterned on the polymer substrate. This can be correlated with a "points per area" as the laser scans back and forth over a specified area. Therefore, laser power and speed control LIG formation at a single laser contact point, while PPI controls how much LIG is produced per area of sample. In summary, PPI, laser power, and etch speed affect how much energy is dissipated through

a given sample area during the LIG production process. How these parameters affect LIG production and RF heating rates will be addressed in this report.

1.2. Polymer Bonding

One potential application that has never been proposed before is the use of LIG as a local heating element to bond polymer surfaces together. Typical bonding of plastic surfaces involves the external application of external heat to the region of interest, which allows for polymer mobility and diffusion across the interface. Prior work in the area of polymer mechanics at interfaces has chiefly focused on "healing" of cut polymer interfaces.[15-20] If two amorphous polymeric bulk samples are brought into contact at an elevated temperature above the glass transition temperature (T_g), the polymer chains diffuse through free chain movement across the interface and increase the entanglement density.[21-24] Reptation theory (originally developed by deGennes) can be used to determine the average interpenetration depth of polymer chains that cross the interface; this results in a scaling law for cohesive tensile strength (σ),

$$\sigma \sim t^{1/4},$$

where t is the exposure time at the heightened temperature.[25,26] At long heating times, this increase in strength would plateau to the bulk polymer value. Prager and Tirrell argue that such scaling arguments do need to be adjusted to account for the high fraction of polymer chain ends near such an interface (in the case of a cut) and the initial configuration of the chains prior to the healing process.[27,28] Similar scaling laws have been applied to healing of semi-crystalline polymers.[26] However, the process of healing interfaces between semi-

crystalline polymers involves melting and re-formation of crystalline regions near the interface.[29] Vogel *et al*. showed (for bulk heating of semi-crystalline polylactide) that the $\sigma \sim t^{1/4}$ scaling does hold. However, the use of localized (rather than bulk) heating of polymer interfaces has not been studied in detail. We hypothesize that the lap shear strength will scale with residence time to the 0.25 power as predicted by theory above. Although the concept of using LIG@polymer (terminology used in this report to describe each sample type) to join polymer surfaces is novel, it is essential to connect the polymer diffusion dynamics to theory using mechanical characterization.

1.3. Nanomaterial Response to RF Fields

Here we focus on the concept of using localized heating at the interface rather than bulk external heating. Several prior studies have investigated the use of nanoparticles as heating elements at interfaces. Both CNTs activated by a microwave field[30-32] and gold nanoparticles (AuNPs) activated by IR light have been investigated for their utility in healing cut interfaces.[29,33,34] These studies have shown substantial increases in strength through the use of these localized heating elements.

In this study, we focus on the concept that local lased and graphitized LIG regions within the polymer may heat when exposed to electromagnetic fields. This is inspired by the numerous reports on rapid heating of sp^2-hybridized carbon nanostructures in response to electromagnetic radiation.[35-43] Previous work from our group has shown that for thermoplastic filaments with a CNT-loaded coating, exposure to microwaves (2.45 GHz)

causes rapid heating of the nanotubes and allows the filaments to be bonded together, which results in improved strength in 3D-printed filament structures.[1]

Most importantly, more recent findings indicate that CNTs also heat in response to frequencies in the 1-200 MHz range.[2] This is a particularly exciting development because RF fields are both safe and versatile, with a number of contact and non-contact applicators that are suitable for industrial scaleup. Recent results for polylactide (PLA) films loaded with multi-walled carbon nanotubes (MWCNTs) are pictured in Figure 1-2, with demonstrations of both contact and non-contact RF heating.[2] As shown in Figure 1-2A, the outer edges of PLA-MWCNT composite films were coated with silver paint to act as electrodes. Alligator clips were then secured to these electrodes in order to supply a sinusoidal RF signal to the sample via a RF signal amplifier. With this setup, one electrode carries the RF signal while the other is grounded, which is an example of contact RF heating.[2] Conversely, the electric fields that are generated between two electrodes may also be used to induce resistive heating in composite films, which is referred to as non-contact RF heating.[2] Figures 1-2B and 1-2C display two possible experimental setups that can produce these electric fields for non-contact RF heating. As shown in Figure 1-2B, a parallel plate system may be used to induce resistive heating, which consists of two copper discs oriented parallel to one another.[2] Similar to the contact setup, one disc is connected to the RF signal amplifier and the other is grounded. The sample is placed between the two discs, as to expose the sample to the electric field generated between these discs. Another example of non-contact RF heating involves a interdigitated fringing-field applicator (Figure 1-2C).[2] For this particular applicator, copper electrodes are laid down

on top of a PI substrate in a serpentine pattern, and the fringing electric field extends above and below these interdigitated electrodes.[2] In both non-contact cases, the coupled electric field induces resistive heating in the samples, rather than a direct RF signal. This setup is similar to the applicator used in this study for characterizing LIG heating ability.

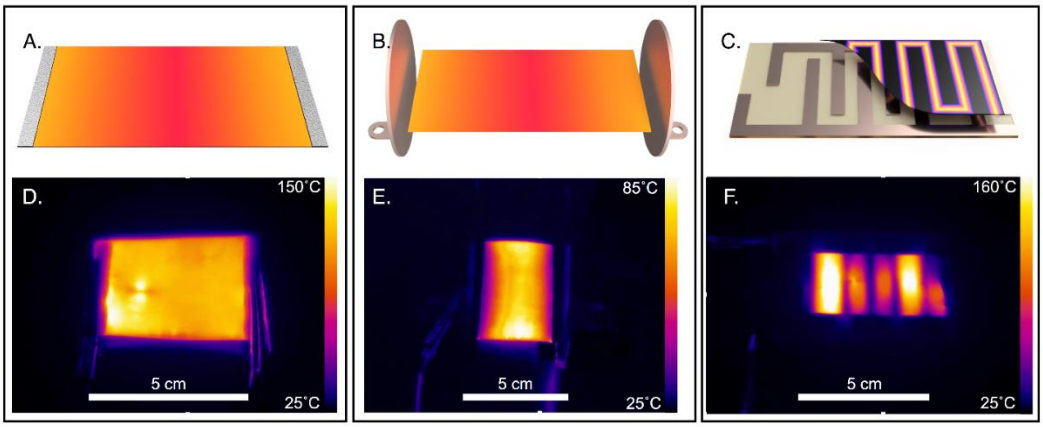

Figure 1-2. Geometry illustrations (top) and corresponding FLIR thermal image (bottom) showing three RF electric field applicator configurations: (A) direct contact, (B) parallel plate, and (C) interdigitated fringing field. These three applicators are applied to three samples: (D) 1.0 wt.% MWCNT in PLA at 315 W, 100 MHz, 4 seconds; (E) 7.5 wt.% MWCNT in PLA at 100 W, 100 MHz, 6 seconds; (F) 1.0 wt.% MWCNT in PLA at 315 W, 50 MHz, 1 second. [Figure and caption reprinted with permission from Green *et al.* Radio frequency heating of carbon nanotube composite materials. *ACS Applied Materials & Interfaces* 2018, *10*, 27252-27259. Copyright 2018 American Chemical Society.]

Regardless of the setup, the CNT-loaded samples exhibited heating rates of 100 ˚C/s when exposed to RF electric fields.[2] Figure 1-2D displays a PLA composite film loaded with 1.0 wt.% MWCNTs exhibiting this resistive heating effect via direct contact. This particular sample was able to reach 150 °C after 4 seconds of RF exposure (315 W of RF power).[2] As shown in Figures 1-2E and 1-2F, non-contact RF exposure resulted in similar magnitudes of RF heating. A 7.5 wt.% PLA-MWCNT composite film was able to

heat up to 85 °C after 6 seconds of RF exposure (100 W of RF power, 100 MHz).[2] Using the interdigitated fringing field applicator, a 1.0 wt.% MWCNT-PLA composite film reached 160 °C in just 1 second of RF exposure (315 W of RF power, 50 MHz).[2] As mentioned previously, the fringing field applicator produces an electric field between the interdigitated copper strips, which results in resistive heating in the sample with a pattern similar to that of the electrode configuration (Figure 1-2F). This type of non-contact applicator is especially useful in our study of LIG RF response, given that LIG composite systems heat especially well in response to fringing electric fields. In addition, one could envision scanning a composite film over the fringing field applicator in order to heat large areas, which could be directly applied to our study of LIG. Our group has already demonstrated how this concept can be used to cure thermosetting adhesives without heating the surrounding matrix.[2]

2. EXPERIMENTAL METHODS

This section details the experimental methods used for this study. As shown in Figure 2-1, the main areas of research in this LIG study include: sample preparation, sample characterization, quantifying RF heating response, sample welding, and 3D printing. Each subheading in Figure 2-1 lists the experimental variables we have explored in this study within each area of research.

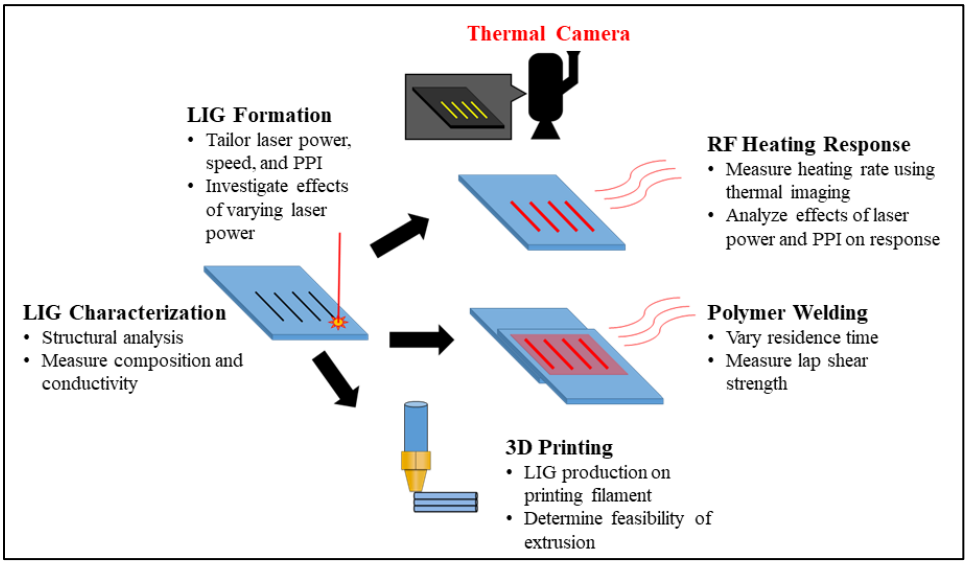

Figure 2-1. Schematic of the main areas of research, which include: sample preparation, sample characterization, determining RF heating response, sample welding, and 3D printing.

2.1. LIG Production on Polymer Substrates

The first step in producing LIG on polymer samples is to properly select the polymer. In this task, we establish a suite of polymers where the heating and welding concepts can be observed. Although Kapton (film, 0.127 mm thick, McMaster-Carr) is a natural choice of model polymer, PESU (film, 0.508 mm thick, CS-Hyde Company) and

PEI (film, 0.508 mm thick, CS-Hyde Company) are actually better choices as our model polymers because of their cross-application to additive manufacturing. In addition to these polymers, we also tested our LIG formation and RF exposure process on PEEK (3D-printing filament, Essentium) and PC (3D-printing filament, Essentium). These choices are based on our preliminary findings, where polymers such as polyamide (3D-printing filament, Essentium) and thermoplastic polyurethane (3D-printing filament, Essentium) did not show LIG formation, while polymers with aromatic groups in the backbone of the polymer (such as PI, PEI, and PESU) did form LIG. Prior to laser treatment, all films and printing filament used for LIG preparation were cleaned with DI water, isopropanol, and additional DI water, respectively. For quantifying RF heating response, 3D Printing filament was cut and pressed into thin films (roughly 0.5 mm thick) using a heat-press machine prior to laser treatment.

A Universal Laser System PLS 6.75 was used for producing LIG on polymer substrates. This is a 75 W, CO_2 laser system that operates at a wavelength of 10.6 μm. This particular system is fit with a motor capable of driving the laser head at a maximum speed of 75 inches per second (in/s) or 1.905 meters per second (m/s). Energy supplied to a given sample area via laser exposure will be varied by controlling the laser power, speed, and PPI. For the RF heating trials, we lase rectangular strips on neat polymer films. For welding trials, we lase multiple parallel stripes (single pass of the laser for each stripe) on the film surface to act as heaters for binding the interface between polymer coupons. Depending on the desired properties, even more complex structures of LIG patterned on

polymer can be created, which creates potential applications for LIG when designing capacitors and other functional materials.

2.2. Characterizing LIG Structures

To confirm that our lasing process produces LIG, we characterize our laser etched samples with Raman spectroscopy. Raman spectroscopy provides information about the LIG composition in terms of number of atomic layers and defect density. Three signature peaks of graphitic structures in Raman spectroscopy are the D peak (~1330 cm^{-1}), G peak (~1600 cm^{-1}), and 2D peak (~2700 cm^{-1}). The ratio of the D to G peak intensity can reveal the existence of defects, including edges and functional groups.[44] The absence of a shoulder in the 2D peak is correlated with few-layer graphene, rather than graphite. The sharpness of the D peak, G peak, and 2D peak can also confirm the formation of graphene, rather than amorphous carbon.[45] Optical microscopy (Olympus BX51) imaging was used to analyze the morphology of LIG as a function of the parent polymer used for LIG formation. Four-point-probe measurements (Keithley 2000) will be used to assess the DC conductivity of the LIG structures.

2.3. Measuring RF Response

In order to test the RF response of LIG@polymer systems, the experimental setup as shown in Figure 2-2 will be used. Radio frequency power (1-100 W, 1-200 MHz) will be applied to the samples with a signal generator (Rigol Inc., DSG815) and 500 W amplifier (Prana R&D, GN500D). A LIG@polymer coupon is laid across two parallel

copper electrodes and secured by two glass slides to a Teflon block coated in dielectric (PI) tape. The electrodes will be connected to the amplifier with a 50-ohm coaxial transmission line terminated by a Type N bulkhead connector with alligator clips soldered to the center pin and ground reference. This setup generates a fringing field that extends above the copper strips (see Section 1.3 for additional details).

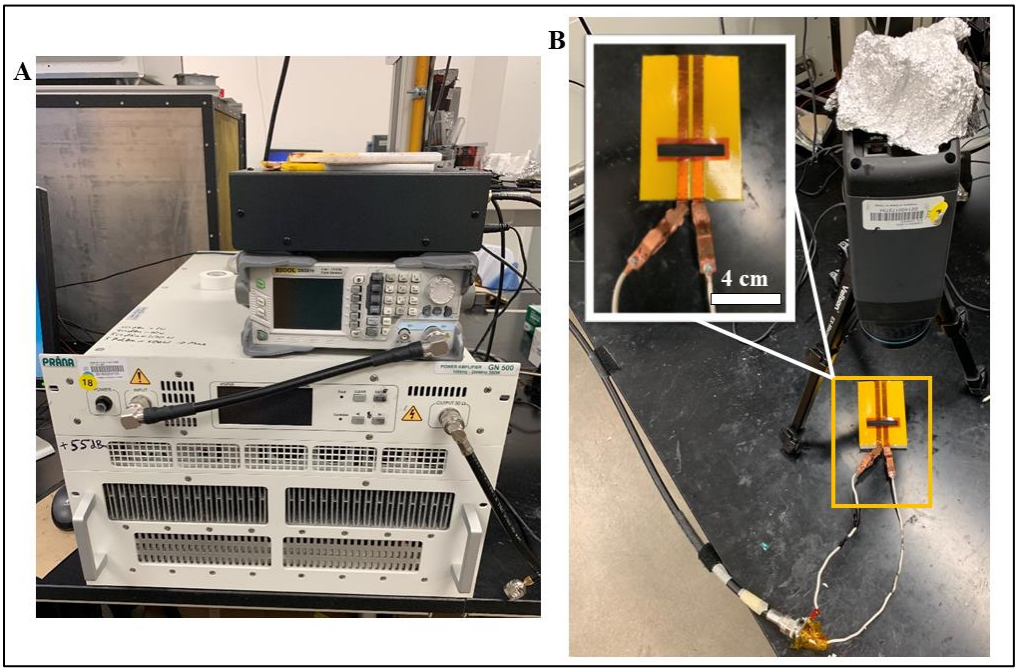

Figure 2-2. (A) Signal generator and amplifier used to produce RF fields. (B) Typical experimental setup for testing the RF field response of each LIG@polymer system. The setup shown here also displays a typical LIG@Kapton sample used for quantifying RF heating.

The two key parameters for the RF field applicator are the power and frequency. The heating rate varies with frequency because of the issue of impedance matching. The LIG@polymer system has both resistance and capacitance, and maximum power is transferred to the system and dissipated as heat when the equivalent load impedance

matches the complex conjugate of the RF source impedance. This impedance matching step can be done through two techniques: (i) by using an auto-tuner for a given frequency, or (ii) by varying the frequency itself until the components are matched. We aim to explore this second area by measuring the frequency-dependent heating behavior of the system.

For each polymer precursor, the heating response of LIG is recorded during RF field exposure using a forward-looking infrared (FLIR) camera system (A655sc, FLIR Systems Inc.) At any point during testing, we may observe the distribution of temperatures present in a particular sample. We also measure the instantaneous heating rate (dT/dt) of the sample using the FLIR camera in order to capture this frequency-dependent heating response as a "thermal spectroscopy" signature. This method was recently developed by our group and provides a rapid, non-destructive way to assess localized heating (and the related complex electrical properties) of LIG@polymer samples.[2] Additionally, long-term heating behavior may be quantified by measuring temperature vs. time for extended times at a single power and temperature.

Using these methods, we explore processing-structure-property relationships for LIG@polymer systems. The processing is defined by both the parameters used to lase the sample (PPI, laser power, etch speed) and the chemical structure of the parent polymer. These factors determine the structure of the LIG@polymer sample: both areal density of LIG spots (PPI) and the depth of the LIG structure (based on laser power/speed and the propensity of the polymer structure to form LIG). Finally, the principal property of interest is the heating response described above, which varies with RF frequency and power.

2.4. Welding Preparation and Mechanical Characterization

After quantifying the heating response of LIG@polymer films, we then apply RF heating of LIG to bond thin films together. The LIG@polymer processing-structure-property relationships described above were then translated to a temperature and time-dependent thermoplastic welding process. The polymer coupon samples are patterned with LIG stripes on its surface as depicted in Figure 2-3A. The spacing and width of the LIG stripes effectively sets the heating element areal density for the weld area. This laser etched coupon is then contacted with a second polymer coupon, also containing LIG (Figure 2-3B). A Teflon block is then placed on top of the stacked LIG@polymer sample to act as a weight and ensure even contact between the top and bottom pieces of the weld sample. Although this process can be applied to a variety of polymers, we use LIG@PEI as our system for welding trials.

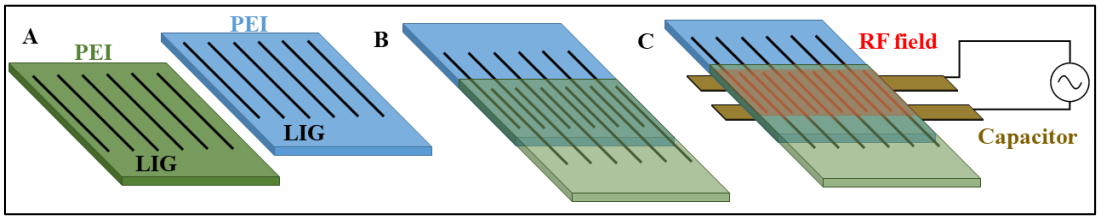

Figure 2-3. (A) To create lap-shear test samples, we use two polymer coupons, each is patterned with LIG stripes using the laser. (B) The coupons are placed in contact with each other prior to being placed atop a capacitor with a fringing RF field. (C) The fringing field will induce heating in LIG and polymer bonding. This allows for rapid, non-contact, non-oven welding.

The sample is then exposed to the RF field at a specified frequency (frequency of maximum heating for that particular LIG@polymer system; addressed in Section 3.2) for a variable time (Figure 2-3C). The weld samples are heated to a target temperature (425

°C) that is comparable to melt processing temperatures of PEI used in additive manufacturing (370-390 °C). The power of the RF field can be modulated to rapidly reach the target temperature within seconds of RF exposure and remain constant.

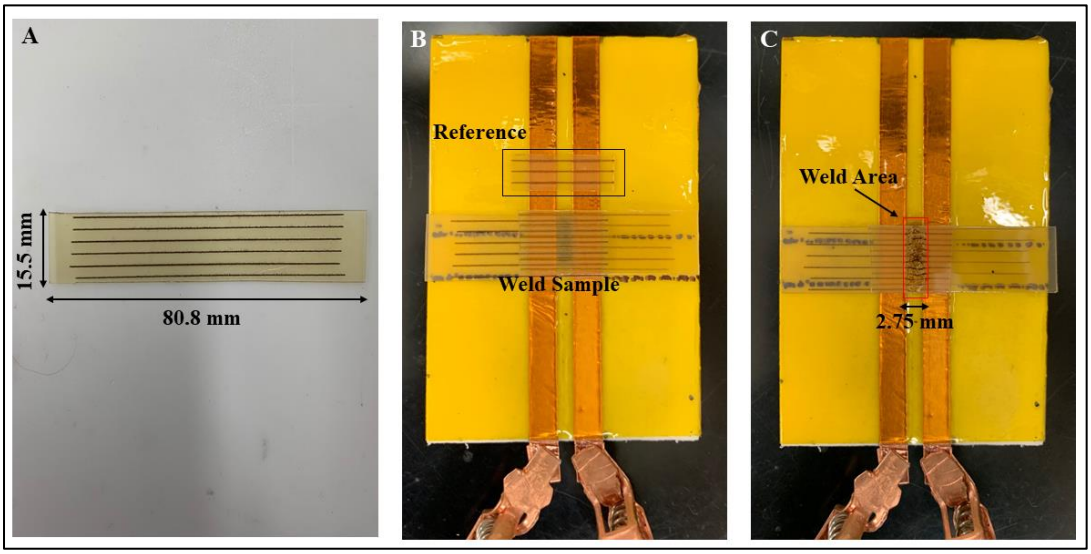

Figure 2-4. (A) PEI film that has been patterned with LIG stripes (5% laser power, 10% etch speed, 1000 PPI). (B) The weld sample is assembled after determining that the bottom coupon and the reference are heating at the same rate. (C) The welded sample has a weld area that is localized between the copper strips and spans over the length of the sample.

Figure 2-4A shows a piece of PEI film that has been patterned with 6 parallel LIG stripes, with each stripe being a single pass of the laser (stripe thickness is roughly 1 mm). This sample is then cut into two pieces or "coupons" and stacked as shown in Figure 2-4B, with the LIG stripes residing in the center of the weld sample. The dotted lines on the applicator are used for positioning the sample, which helps limit variability in heating behavior between weld samples. Figure 2-4C shows two LIG@PEI coupons welded together after RF exposure. The weld forms along a single line between the copper strips,

which corresponds to the fringing field center (where the field is most powerful). It is possible to scan the samples over the center of the RF field and weld larger areas, but for proof of concept we use stationary samples.

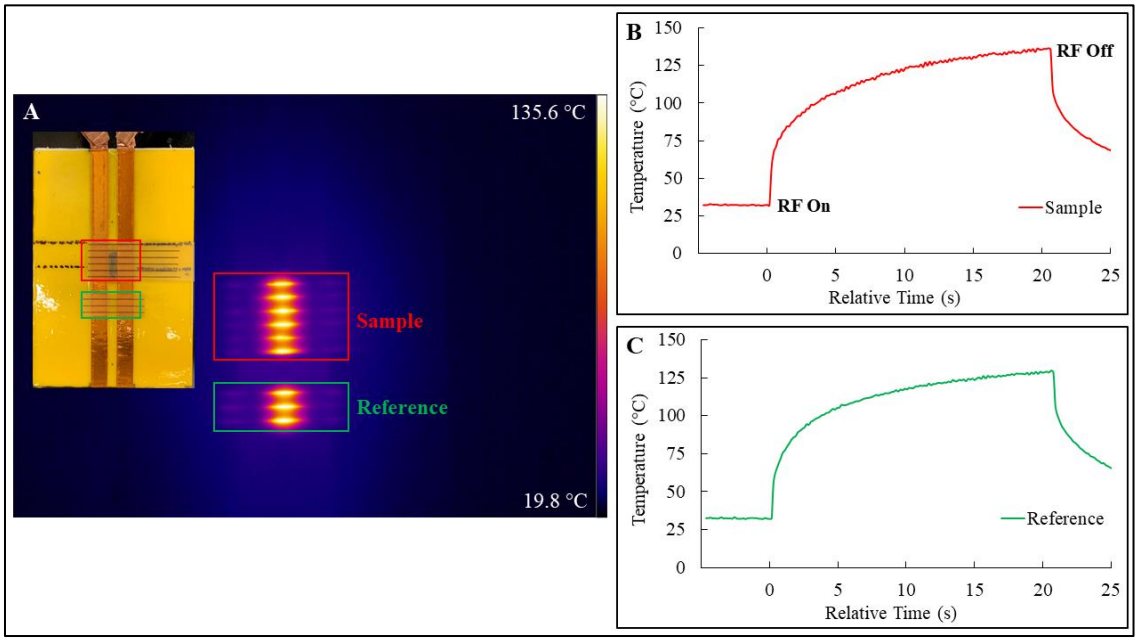

Figure 2-5. (A) FLIR image that was captured after 20 s of RF exposure (103 MHz, 2.0 W). An image showing the sample and reference orientation with respect to the RF applicator is also included (both prepared with 5% laser power, 10% etch speed, 1000 PPI). (B/C) Plots showing the maximum temperature of the weld sample (B) and reference (C) recorded by the FLIR camera over time. In these plots, time "0" corresponds to the moment when the RF field was engaged.

Due to the fact that the weld sample is covered with a Teflon block during welding, we use a reference sample placed parallel to the weld sample in order to estimate the temperature distribution in the weld sample (Figure 2-4B). The FLIR software can monitor the temperature of the uncovered reference sample in real-time, which is heating at the same rate as the weld sample (Figure 2-5B/C). To confirm that the reference and weld

samples are heating at the same rate, we compare the RF response of the bottom coupon of the weld sample versus the reference at low RF power (2.0 W). After confirming that both samples are heating comparatively, the weld sample is assembled and RF power is increased until the target temperature is reached. We then vary the amount of time that the weld sample is exposed to RF, as is addressed in Section 3.3.

Weld samples were prepared with varying RF exposure time with the goal of quantifying the relationship between lap shear strength and exposure time. Lap shear testing was performed using an MTS Insight electromechanical testing system fit with a 30 kN load cell and pneumatic test grips (40 psi). For each test, a uniaxial constant load is applied to the weld at a rate of 0.05 in/min (1.27 mm/min). The fracture strength is calculated as the load when the weld fails divided by the weld area (15.5 mm by 2.75 mm) depicted in Figure2-4C. Additional lap shear testing information is provided in Section 3.4.

2.5. Printing with LIG Filament

Finally, we aim to determine how LIG@polymer composites may function in an industrial setting, with particular application to additive manufacturing and functional coatings. We intend to prove that LIG may be used in 3D printing as a means of improving the weld strength of various thermoplastic parts. For this portion of the study, we chose PEI (Ultem 1010, 1.75 mm diameter, 3DXTech) and PESU (1.75 mm diameter, 3DXTech) as the model polymers for this application, given that they are commonly used in additive manufacturing. First, we pattern the exterior of the printing filament with LIG,

as shown in Figure 2-6. After printing a part, the LIG stripes will act as local heating elements for welding 3D-printed filament traces together and improving the isotropic strength of 3D-printed structures. All printing will be completed with an Intamsys Funmat HT Enhanced Printer, located in the Green lab. We aim to show that the LIG@polymer filament can indeed be extruded and retain RF responsiveness and electrical conductivity post-print.

Figure 2-6. A prototype LIG@PESU printing filament developed at TAMU (5% laser power, 10% etch speed, 1000 PPI). Filament diameter is 1.75 mm, typical for material extrusion 3D printers.

3. RESULTS

Our results indicate that we can produce RF responsive, graphitic structures from Kapton, PEI, PESU, PEEK, and PC using the experimental methods detailed above. In addition, the RF heating rate of each LIG@polymer sample has been quantified. The effect of RF field power on LIG heating has also been analyzed. We have investigated the effects of PPI and laser power on LIG structure and RF field response. We also find that these LIG structures may be used for welding polymer interfaces, and that weld strength depends on the RF field exposure time. In the following sections, the results that have been obtained thus far are summarized.

3.1. LIG Formation and Characterization

RF responsive, graphitic material was successfully produced from a variety of industrially relevant thermoplastics via laser etching. The laser parameters (power, speed, and PPI) used in the initial stages of this study were derived from previous work completed by Tour *et al*. on LIG formation.[11,13] Slight adjustments were made to these laser parameters as needed based on the equipment available at Texas A&M. The optimized laser parameters used for quantifying RF heating rates for each LIG@polymer system may be seen in Table 3-1. Note that the parameters may be reported as a percentage of the maximum power output (75 W) and maximum etch speed (1.905 m/s) of the PLS 6.75 laser system.

	Kapton	PEI	PESU	PEEK	PC
Laser Power (%)	30 (22.50 W)	5 (3.75 W)	5 (3.75 W)	5 (3.75 W)	3-1x (2.25 W), 5-1x (3.75 W)
Laser Speed (%)	50 (0.95 m/s)	10 (0.19 m/s)	10 (0.19 m/s)	5 (0.09 m/s)	10 (0.19 m/s)
Points per Inch (PPI)	1000	1000	1000	1000	1000
Total Number of Lases	1	1	1	2	2

Table 3-1. Optimized laser parameters used to prepare each LIG@polymer system for quantifying RF heating rates.

Choosing the correct laser power and speed is imperative for producing RF responsive, graphitic material. Although each parameter is controlled individually, LIG production and the resulting RF response is dependent on all three parameters (power, speed, and PPI). As stated previously, these parameters ultimately control the laser energy dissipated per area of material during laser etching. The versatility of this method allows us to spatially pattern LIG on polymer substrates via CAD designing, as shown in Figure 3-1. This image illustrates that intricate designs may be produced using this process.

Figure 3-1. A 76.2 mm x 76.2 mm sample of Kapton that has been etched by a CO_2 laser (30% laser power, 50% etch speed, 1000 PPI). The pattern displayed was designed prior to lasing using AutoCAD.

In order to confirm that our laser etching process indeed forms LIG, Raman spectroscopy was performed on LIG@Kapton. We observe three distinct peaks (D, G, and 2D) in the spectrum for this system, which may be seen in Figure 3-2. The D peak appears at 1352 cm^{-1}, the G peak at 1580 cm^{-1}, and the 2D peak at 2678 cm^{-1}. The shape of the spectrum is consistent with graphitic material produced via laser etching.[11] The sharpness of the D peak, G peak, and 2D peak also suggest the formation of graphitic material, rather than amorphous carbon.[45] However, the intensity of the D peak relative to the G peak suggests that LIG produced via laser etching may possess some defects (edges, functional groups, incomplete sp^2 character). The shoulder on the left side of the 2D peak also suggests that our product is structurally similar to that of multilayer graphite, as opposed to single-layer graphene.[44]

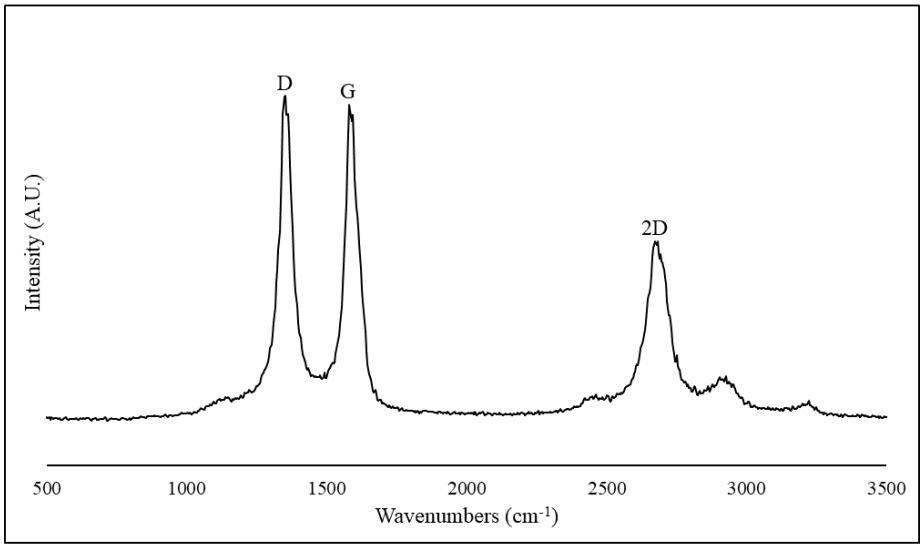

Figure 3-2. Raman spectrum of LIG@Kapton (excitation wavelength = 532 nm). We observe three distinct peaks: D (1352 cm^{-1}), G (1580 cm^{-1}), and 2D (2678 cm^{-1}).

We use optical microscopy to further investigate the LIG formation process and determine the effects of each laser parameter on LIG structure. As stated in Section 2.1, we lase rectangular strips on neat polymer films for the initial RF heating trials (Figure B-1 shows this sample geometry). To produce these samples, the laser starts at the top right corner of the sample design and moves linearly across the entire width of the sample, which makes up a single "pass" of the laser. The laser then moves in the negative y-direction, and completes another pass in the x-direction. This process is repeated until the entire sample design is completed. It should be noted that the laser fires only when prompted by the AutoCAD design, and uses 1000 PPI automatically when lasing large areas. The optical microscopy images of LIG@PEI and LIG@PESU shown in Figure 3-3 display the morphology of these lased areas. The dark regions in these images correspond to LIG, while the lighter regions are the parent polymer that was not converted to LIG

during the laser etching process. The pathway of the laser is apparent in these images, which suggests that multiple lases may be required to fully convert a polymer surface into LIG. However, this point was not explored in this study. Despite the apparent porosity of these samples, LIG connectivity was sufficient enough to act as a conductive material and induce heating when exposed to RF fields. We find that LIG possesses a DC conductivity of 5800 S/m, which is comparable to values reported in literature.[11,12]

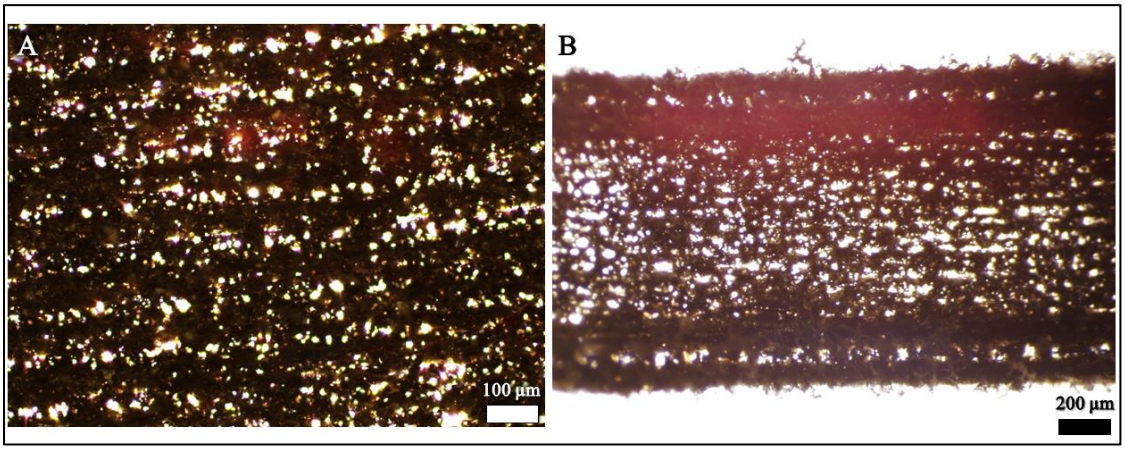

Figure 3-3. Optical microscopy images taken of (A) LIG@PEI (scale bar=100 µm) and (B) LIG@PESU (scale bar=200 µm) stripes. The dark regions are LIG, while the light regions are areas of the parent polymer that were not converted to LIG during the laser etching process. Both samples were prepared with 5% laser power, 10% etch speed, and 1000 PPI.

As stated previously, PPI controls the spacing between laser contact points, which can be correlated to laser contact points per area. Reducing PPI decreases the number of laser contact points per area of sample. Therefore, we believe that decreasing PPI will reduce the amount of LIG that is produced per area of precursor material during laser etching. The laser system used in this study can etch samples with a PPI ranging from 10-1000. To test our hypothesis, we prepared LIG@PEI samples with varying PPI (100 to

1000 in increments of 100). In order to control PPI, we must use a sample geometry that only uses single passes of the laser (Figure B-2), which is one limitation of the laser system used in this study. As stated previously, prompting the system to continuously lase a large area (as is the case with the RF heating samples in Figure B-1) automatically sets the PPI to 1000. In order to determine how PPI affects LIG production, optical microscopy was performed on these samples. Figure 3-4 shows a single pass of the laser on PEI produced with 1000 PPI versus 300 PPI. As shown in Figure 3-4A, we find that a single laser pass produces two stripes of LIG with unconverted polymer between the stripes. When compared to the 1000 PPI sample, the amount of LIG produced in the 300 PPI sample (Figure 3-4B) is much lower, indicated by the increased transparency of the stripe. Therefore, one can effectively control how much graphitic material is produced in a given sample by altering laser PPI. In Section 3.2, we investigate the effects of PPI on RF response.

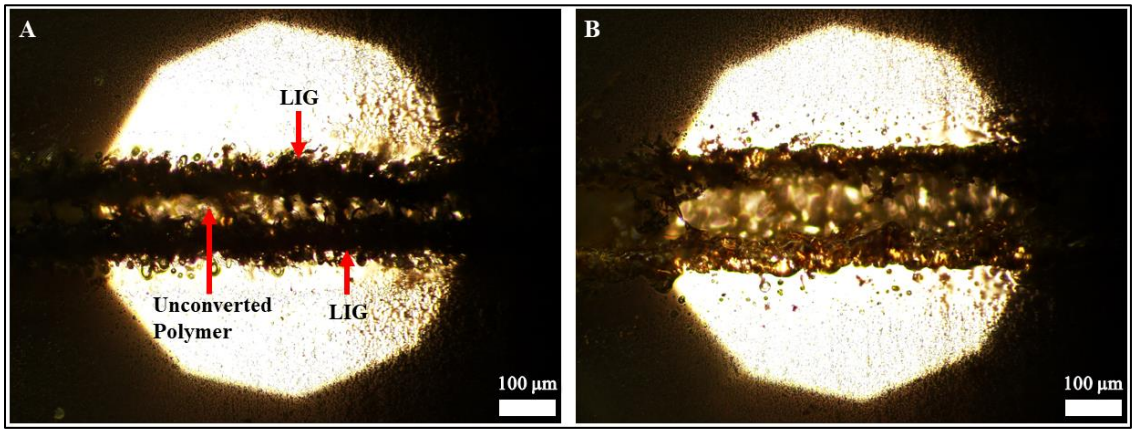

Figure 3-4. Optical microscopy images (scale bar=100 µm) of a single laser pass on PEI produced with 1000 PPI (A) and 300 PPI (B). 5% laser power and 10% etch speed were used in both cases.

We also investigate the effects of treating LIG@polymer systems with mild organic solvents, such as isopropanol. For this study, we take a LIG@Kapton sample and cover it with a Kimwipe that has been wetted with isopropanol. We allow the sample and Kimwipe to remain in contact for roughly 5 seconds, long enough for the isopropanol to wet the LIG@Kapton sample. After removing the Kimwipe and allowing the isopropanol to evaporate from the sample, we took optical microscopy images and tested the RF response of the solvent-treated sample. Figure 3-5 shows a LIG@Kapton sample before (Figure 3-5A) and after (Figure 3-5B) solvent treatment. As was also the case in Figure 3-3, the pathway of the laser is apparent in the unaltered sample. It appears that solvent treatment effectively removes this structural characteristic and increases LIG surface coverage. The solvent treatment allows for LIG agglomeration due to capillary effects during solvent evaporation, thus increasing density and decreasing porosity. How this affects the RF response of LIG@Kapton samples will be discussed in Section 3.2.

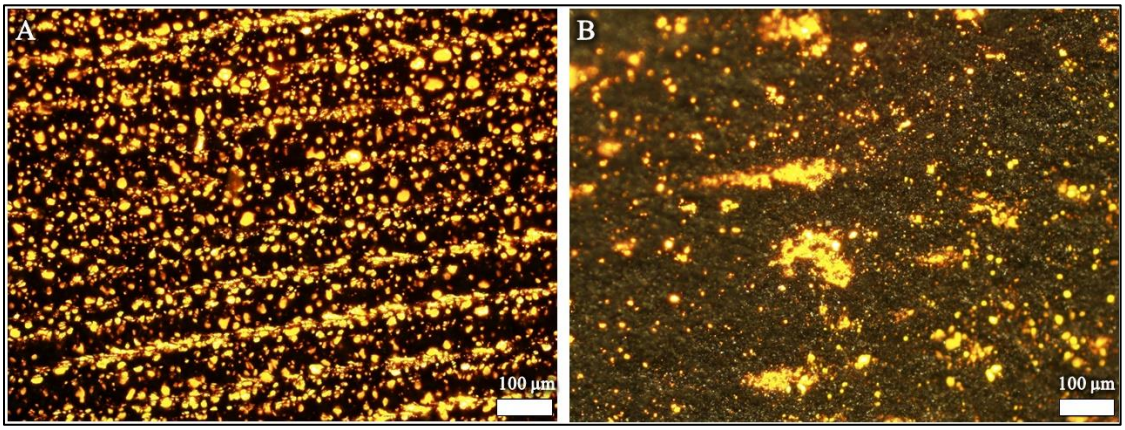

Figure 3-5. Optical microscopy images (scale bar=100 µm) taken of a single LIG@Kapton sample (30% laser power, 50% etch speed, 1000 PPI). (A) The unaltered sample (after laser treatment) clearly shows the pathway of the laser and resulting porous LIG structure. (B) After solvent-treating the LIG regions in (A), porosity is reduced and LIG connectivity increases.

3.2. LIG@Polymer RF Heating

Through this study, we have demonstrated that RF responsive, graphitic material may be produced from a variety of commodity plastics. Using the experimental setup displayed in Figure 2-2, we may effectively measure the heating response of LIG to RF fields. In order to quantify the heating response of LIG, we perform RF field frequency sweeps on each LIG@polymer system. We expose the sample to RF fields with frequencies ranging from 50 to 145 MHz at a constant power of 10 W. This range of frequencies was chosen based on previous work from our group (rapid heating of MWCNT's) and preliminary results which suggested LIG was responsive in this range.[2] During this test, samples are exposed to RF fields for 5 seconds at each frequency increment (whole number values only) within the specified range. This test allows us to determine the frequency of the RF field that induces maximum heating rates in each LIG@polymer sample. The RF heating response of LIG@Kapton may be seen in Figure 3-6. The FLIR image in Figure 3-6A shows an instantaneous temperature distribution across a LIG@Kapton sample during a frequency sweep. The hottest region of the sample is localized between the two copper strips, where the RF field is strongest. Figure 3-6B displays heating rates of the LIG@Kapton sample shown in Figure 3-6A as a function of RF field frequency. Particular resonant modes can be seen; these are the frequencies where resistive heating is highest and reflected power is lowest.

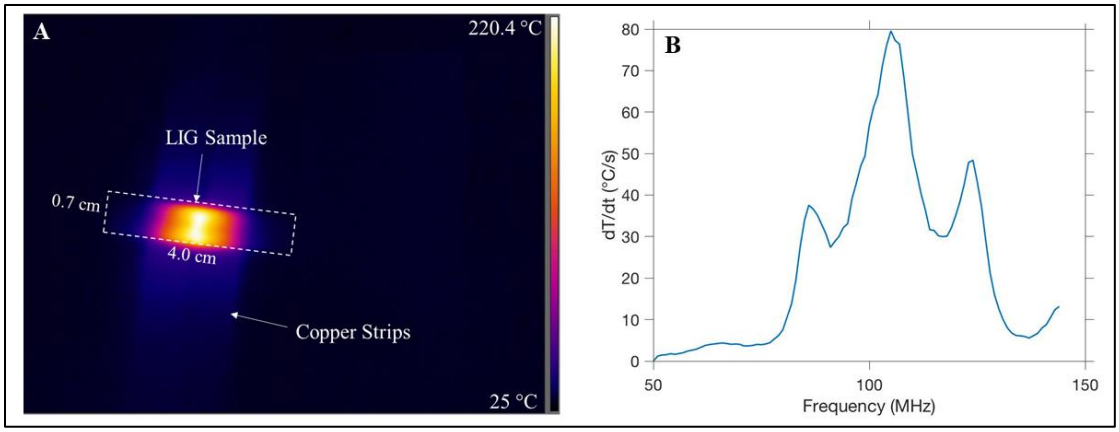

Figure 3-6. (A) Temperature distribution across a LIG@Kapton sample during RF field exposure (30% laser power, 50% etch speed, 1000 PPI). (B) Heating response of the sample in (A) as a function of the frequency of the applied RF field. The power of the RF field in both cases was 10 W.

Regardless of the parent polymer used to produce LIG, these resonance modes are present among each LIG@polymer system that was tested (see Figures A1-A4). As a result, we believe that this is characteristic of LIG RF heating response, given the experimental setup that was used. However, we find that maximum heating rate varies across each system, as shown in Table 3-2. This variability is caused by differences in LIG content and long-range connectivity between each system. We believe that the amount of LIG, as well as connectivity between LIG regions, produced during laser treatment has a direct effect on instantaneous heating rates, with higher LIG content and connectivity corresponding to larger heating rates. Regardless, these instantaneous heating rates are quite high and indicate that rapid, on-demand heating inside polymer structures is possible. Table 3-2 also shows the RF field frequency required to achieve the maximum heating rate of a particular LIG@polymer system. We find that LIG RF heating response is

greatest in the range of 100-120 MHz, regardless of the parent polymer used to product LIG.

	Kapton	PEI	PESU	PEEK	PC
Maximum Heating Rate (°C/s)	79.55	106.75	122.45	20.99	49.35
RF Field Frequency (MHz)	105	103	114	106	108

Table 3-2. Maximum heating rates for each LIG@polymer system observed during RF frequency sweeps at a constant power of 10W. The frequencies which induced maximum heating rates for all systems are also shown. The laser parameters used to prepare these samples are listed in Table 3-1.

As stated previously, the strength of the RF field also plays an important role in localized heating of nanomaterials. To quantify this effect for LIG, we measure steady state temperature as a function of RF power in LIG@Kapton samples at a fixed frequency (Figure 3-7). In most cases, LIG reaches a steady state temperature in about 30 seconds of constant RF exposure. As shown in Figure 3-7, LIG steady state temperature increases linearly with RF power up until about 2 W. Above 2 W, the rate at which temperature increases with RF power starts to decline. At 25 W of RF power, LIG can reach localized temperatures upwards of 560 °C. This was the highest RF power tested, as Kapton films tend to thermally degrade above these temperatures. Based on the trend in Figure 3-7, we believe that steady state temperature would eventually reach a maximum at high RF powers. In summary, the RF heating response of LIG can be fine-tuned to a specific

temperature, which could be quite useful for curing epoxies or welding polymer interfaces (Section 3.3 reviews the latter).

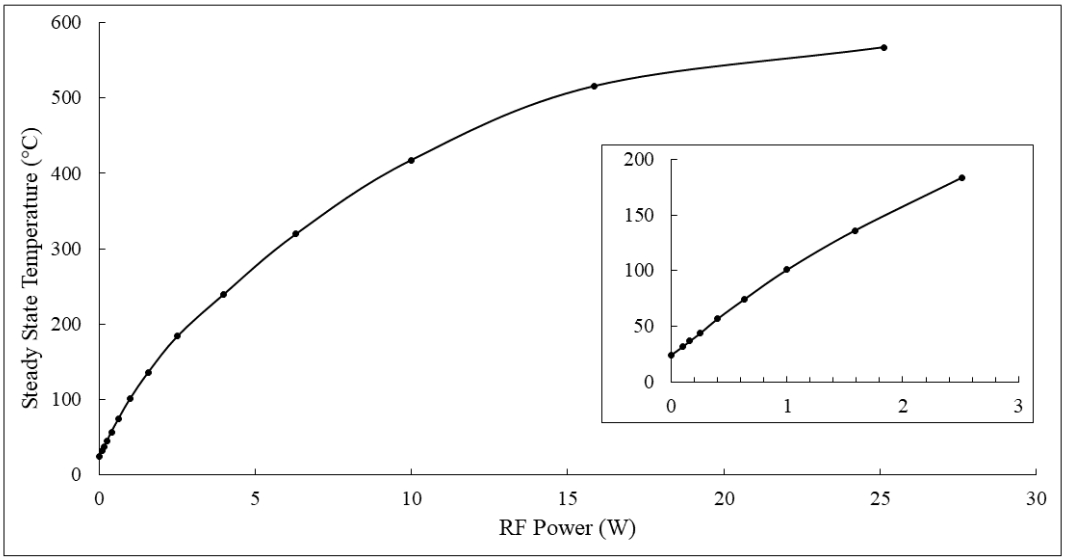

Figure 3-7. Plot showing steady state temperature as a function of RF power in LIG@Kapton samples (30% laser power, 50% etch speed, 1000 PPI) during constant RF exposure (fixed frequency of 105 MHz).

In order to test our theory about LIG content and connectivity affecting RF response, we investigate the effects of PPI on the RF heating response of LIG@polymer systems. As is detailed in Section 3.1, PEI was used as the polymer precursor for this study. Each sample was prepared with the same laser power (5%) and etch speed (10%) while varying PPI. To gauge the RF response of each sample, we record the maximum temperature across the sample during 5 seconds of RF field exposure (10 W of Power, 103 MHz). Figure 3-8 shows a plot of these temperatures as a function of PPI. A distinct transition occurs in RF response between 700 and 600 PPI, where maximum temperature drops from 358.1 to 52.1 °C. In order to obtain a better idea as to when this transition

occurs, we also tested the RF response of LIG@PEI samples prepared with 675, 650, and 625 PPI. These results show that LIG connectivity drops below the percolation threshold at 650 PPI. Below the percolation threshold, RF response is significantly weaker due to the lack of long-range connectivity between LIG regions. The RF field heating effect is completely lost at 300 PPI, which meant that lower values of PPI need not be tested. Above the percolation threshold, RF response decreases with PPI. Additional optical microscopy images of these PPI trial samples are provided in Appendix B (Figure B3-B8). These images show that the amount of LIG produced in a single pass of the laser decreases as PPI decreases. Lowering the number of laser contacts within a certain area means that less neat polymer will be converted to LIG, thus decreasing RF response.

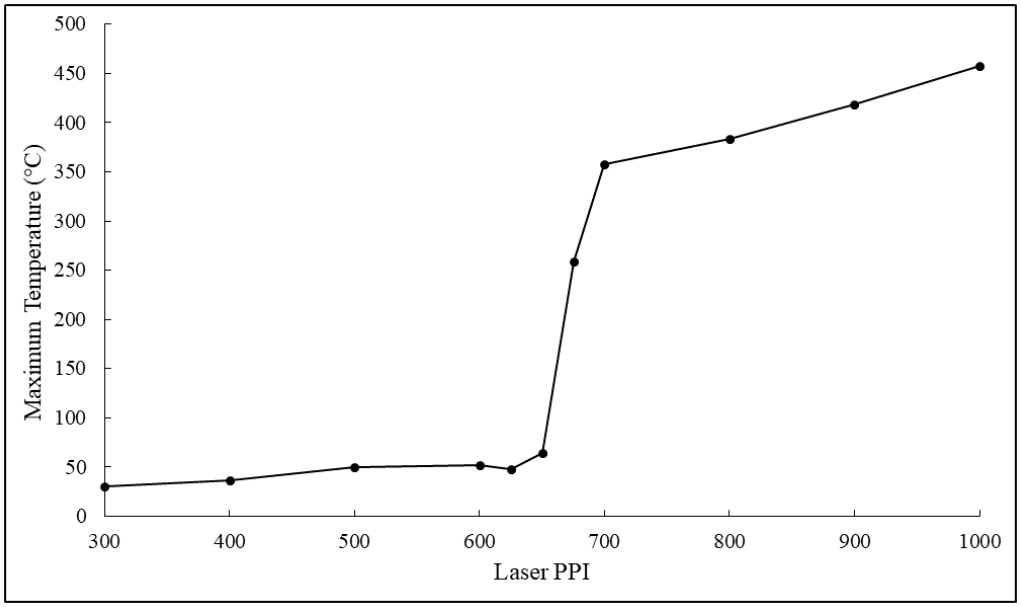

Figure 3-8. Plot displaying maximum temperature at 5 seconds of RF exposure (10 W of Power, 103 MHz) as a function of laser PPI on LIG@PEI (5% laser power, 10% etch speed, 1000 PPI).

In addition to laser PPI, we also investigated the effects of laser power on RF heating of LIG@PEI. Tour *et al.* states that LIG formation is possible at higher laser powers (higher than those listed in Table 3-1), and that increasing laser power increases the porosity of the resulting LIG structure.[11] To test RF response as a function of laser power, we prepared LIG@PEI samples (rectangular strips like those displayed in Figure B-1) with 5, 7, and 10% laser power while keeping etch speed (10%) and PPI (1000) constant. As shown in Figure 3-9, temperature was measured over 30 seconds of constant RF exposure (10 W of Power, 103 MHz) for each sample. We find that LIG@PEI samples prepared with the optimized laser parameters in Table 3-1 possess the greatest RF response, and that RF response decreases with increasing laser power. To understand why this happens, optical microscopy was performed on each sample (Figure B9). These images show that the microstructure of the 10% sample is significantly different from the 5% and 7% samples. At this point, we are not exactly sure why the 10% samples possess this structure. However, we can confirm that LIG is still being formed at 10% laser power, given that these samples were RF responsive. One idea is that the excess laser energy is sufficient enough to melt the neat polymer surrounding the LIG regions. Upon melting, the neat polymer would encapsulate the LIG, thus disrupting long-range connectivity between LIG regions and reducing RF response. To confirm or deny this theory, we can perform TGA on each of these samples. Graphene typically decomposes around 700-800 °C, so any significant weight loss below this temperature range would confirm the presence of neat polymer and our theory about LIG encapsulation during laser exposure.

In summary, supplying excess laser energy to the sample during LIG production can diminish RF response.

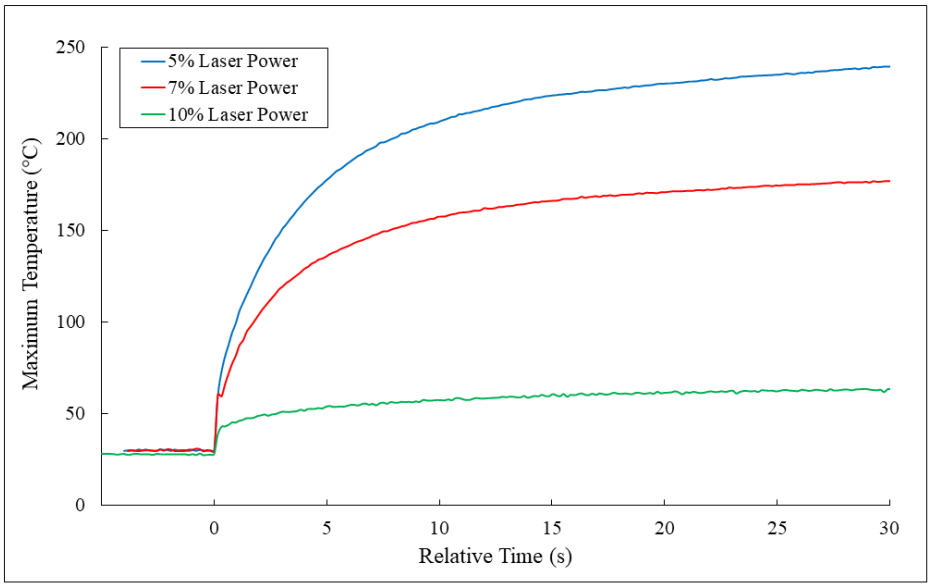

Figure 3-9. Plot displaying temperature over 30 seconds of constant RF heating (10 W of Power, 103 MHz) for samples prepared with 5% (blue), 7% (red), and 10% (green) laser power (10% etch speed and 1000 PPI used in all cases). Time "0" corresponds to the moment when the RF field was engaged.

As described in Section 3.1, we found that treating LIG@Kapton samples with mild solvents, such as isopropanol, reduces LIG porosity. We also tested the RF response of these samples to determine if solvent treatment affected the heating ability of LIG. Figure 3-10 shows FLIR images of unaltered LIG@Kapton and solvent-treated LIG@Kapton captured after 30 seconds of RF heating. Both samples show similar temperature profiles, which suggests that exposing LIG to mild solvents does not diminish RF response. In fact, the solvent-treated sample heated marginally faster than the untreated sample when exposed to RF fields. The reduction of LIG porosity after solvent treatment

was most likely the cause of this slight increase in RF heating ability. This finding has substantial relevance for solvent casting polymer-based films on top of LIG structures. One could imagine casting a solution containing neat polymer on top of a LIG@polymer sample. As the solvent evaporates, LIG would become embedded in the drying film. After drying, the film would contain RF responsive nanofiller, which could be used as a new method for preparing nanocomposites.

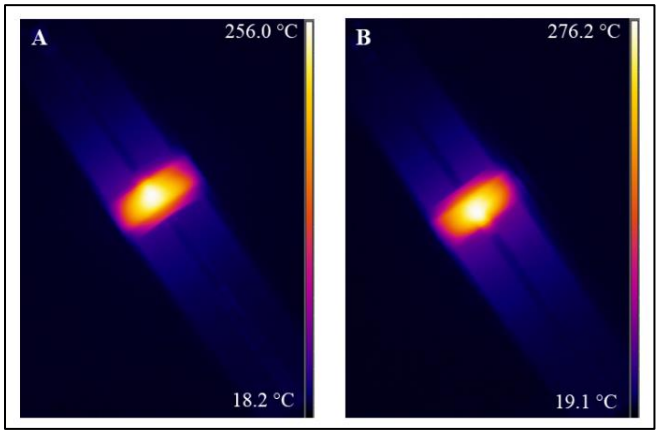

Figure 3-10. Thermal image of unaltered (A) and solvent-treated (B) LIG@Kapton during RF exposure (30% laser power, 50% etch speed, 1000 PPI). Temperature profiles show the maximum temperature reached in 30 seconds of RF heating (10 W of Power, 105 MHz).

3.3. Rapid Welding of Polymer Surfaces

As detailed in section 2.4, we use LIG to weld polymer surfaces together using RF heating. To determine the relationship between RF exposure time and lap shear strength, we prepare LIG@PEI weld samples (Section 2.4) with varying RF exposure time. We find that localized temperatures ranging from 375-425 °C are sufficient to weld LIG@PEI samples, while LIG@PESU samples require localized temperatures ranging from 350-400

°C. In the interest of forming a solid weld as quickly as possible, we chose our target temperature to be 425 °C for LIG@PEI. Although this welding procedure also works for LIG@PESU, we chose LIG@PEI as the model system for exploring the relationship between exposure time and weld strength. As stated previously, RF power is increased until the target temperature is reached, which is then maintained by modulating power. RF power modulation helps mitigate thermal degradation in the neat polymer surrounding the LIG regions by preventing localized temperatures from exceeding far beyond the target temperature. For example, if weld temperature exceeds 475 °C for extended periods of time during LIG@PEI weld sample preparation, lap shear strength decreases due to thermal degradation. The same is true for LIG@PESU samples when the local temperatures exceed 400 °C.

During weld trials, RF exposure time was varied between 30 and 150 seconds in increments of 30 seconds. Localized temperatures were monitored using a FLIR camera during all sample preparation. It is common for temperature to fluctuate during RF exposure when preparing samples; this is simply the nature of RF heating and the RF setup used in this study. RF power modulation helps to control these temperature fluctuations. Table 3-3 provides a summary of lap shear strength of welded LIG@PEI coupons as a function of RF exposure time. A graphical representation of this data is provided in Appendix A (Figure A-5).

Exposure Time (s)	Weld Strength (MPa)
30	8.92 ± 0.29
60	10.19 ± 0.56
90	11.81 ± 0.74
120	12.74 ± 0.66
150	12.86 ± 1.57

Table 3-3. Average weld strength of welded LIG@PEI coupons at various RF exposure times. Samples were prepared as depicted in Figure 2-4.

Each data point shown in Table 3-3 is an average of five test samples. Variability within each data set was most likely caused by temperature fluctuations when making the samples, which can affect the quality of the weld. RF power modulation allows us to control the maximum temperature in the sample, but in some instances the temperature distribution across LIG regions can vary. Nevertheless, these results show that weld strength increases with RF exposure time. Increasing the RF exposure duration allows more time for polymer chains to diffuse across the weld interface and become entangled, thus creating a stronger weld. Additional images of LIG@PEI welded samples are provided in Figure 3-11.

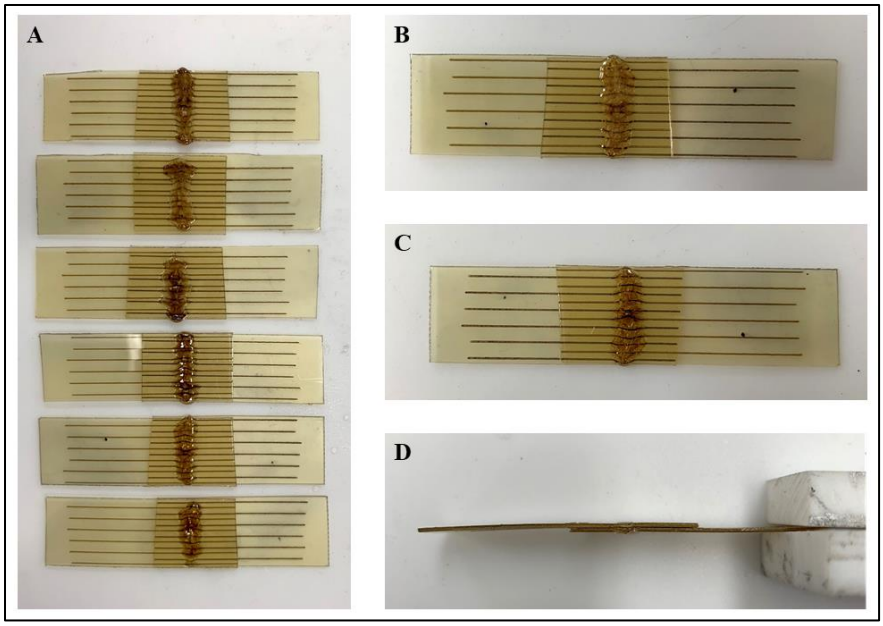

Figure 3-11. (A) A set of LIG@PEI welded samples. This image shows that weld area is consistent, suggesting that this RF welding process is reproducible. (B-D) Images of a single LIG@PEI sample, showing top (B), bottom (C), and side (D) views.

To determine if this data agrees with the scaling law for cohesive strength (σ), which says that cohesive strength scales with time to the 0.25 power, we plot these points on a logarithmic scale (Figure 3-12).[25,26] As shown in this plot, weld strength scales with RF exposure time to the 0.244 power. This suggests that the scaling law for cohesive strength indeed applies to RF welding of amorphous polymer interfaces. Given these results, we hypothesize that weld strength will eventually reach a maximum at long RF exposure times (greater than 150 seconds), in accordance with theory.[25,26]

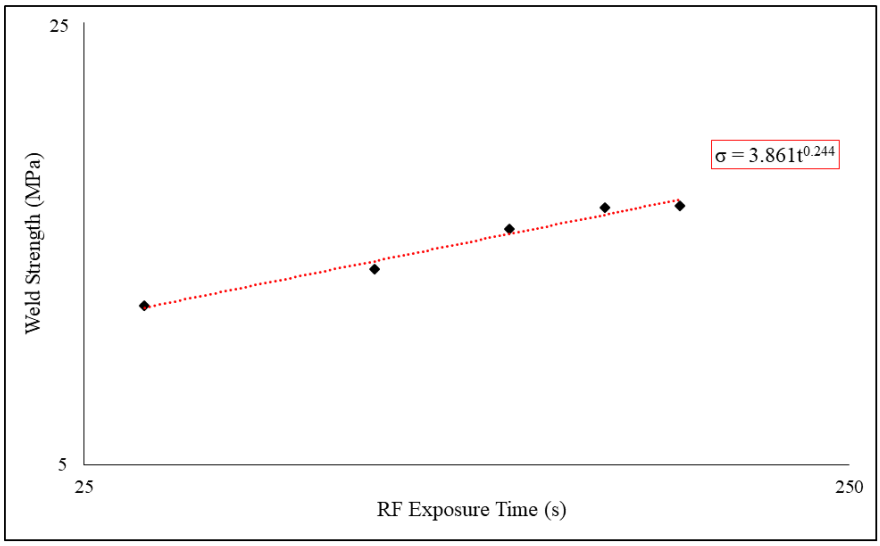

Figure 3-12. Weld strength as a function of RF exposure time plotted on a logarithmic scale. The red dotted-line represents the trendline for this data set.

To better understand how LIG morphology changes during welding, we perform optical microscopy on LIG@PEI coupon surfaces (Figure 3-13). These images show a single LIG stripe on PEI after welding and lap shear testing. The region that surrounds each LIG stripe is the previously melted polymer resulting from rapid heating during welding. These results prove that LIG becomes encapsulated in the molten polymer during welding, given that LIG stripes remain structurally intact even after shear failure. However, air can be trapped in the molten polymer during welding, which results in the formation of bubbles (Figure 3-13A).

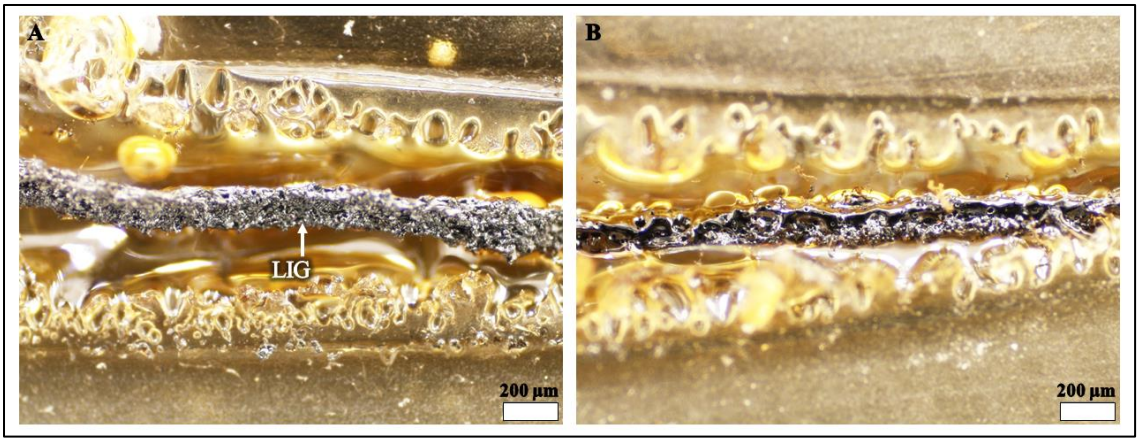

Figure 3-13. (A/B) Optical microscopy images (scale bar=200 µm) of LIG@PEI stripes after welding and lap shear testing. The structural integrity of LIG stripes is maintained throughout the welding process.

3.4. Additive Manufacturing

We have demonstrated that LIG may be used as a local heater in polymer-based systems when exposed to RF. We find that this method may be useful in additive manufacturing, with a focus in alleviating residual stresses and increasing isotropic strength of various 3D-printed parts. As shown in Figure 3-14, the laser etching process may be applied directly to PI printing filament. In just 5 seconds of RF field exposure (10 W power), localized temperatures of 228.8 °C may be achieved. Similar values have also been seen for LIG@PEI and LIG@PESU printing filament after laser etching. Preliminary results suggest that LIG is printable, which becomes embedded in molten polymer as it is extruded during printing. RF responsiveness is retained post-print, meaning that LIG may be used as a means of increasing weld strength after printing a part through rapid heating.

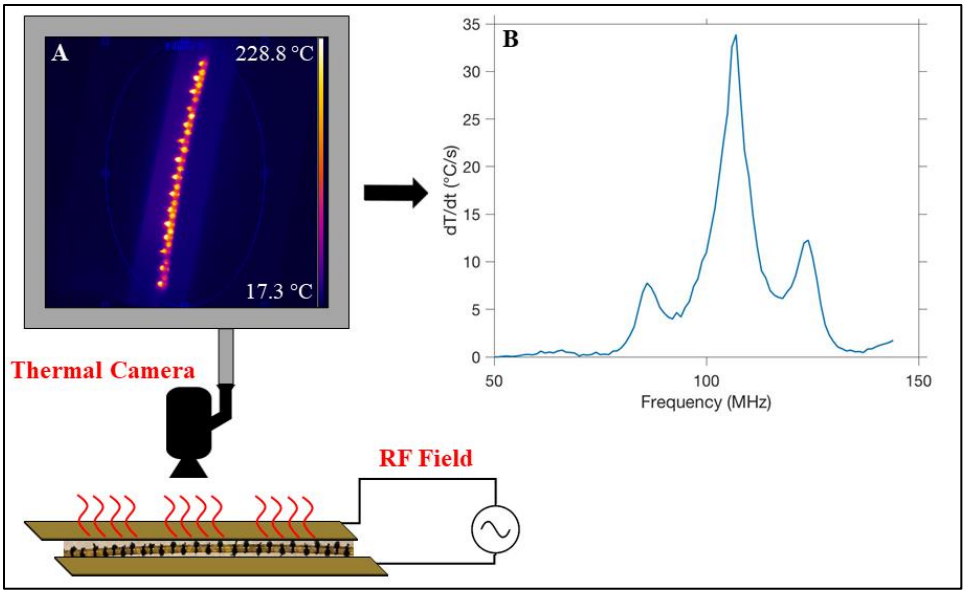

Figure 3-14. (A) Thermal image of LIG@PI filament during RF field exposure (30% laser power, 50% etch speed, 1000 PPI). (B) Heating rates up to 34.5 °C/s allow for rapid heating of LIG@PI filament pre and post print.

4. CONCLUSIONS AND FUTURE WORKS

At the current stage of this study, we have demonstrated that graphitic structures may be produced using a conventional laser cutting system. We also find that these graphitic structures rapidly heat when exposed to electromagnetic energy via RF fields with exceptionally high heating rates (up to 124 °C/s). RF heating response depends on the parent polymer used to produce LIG, in that, some polymer precursors are more susceptible to forming LIG than others when exposed to CO_2 lasers. Our results also show that LIG heating response depends on RF field power, as steady state temperatures increase as RF power increases.

We find that LIG morphology and RF heating response is affected by laser power and PPI. Using excess laser power to produce LIG has been proven to reduce rapid heating ability. Excess laser power seems to affect LIG morphology as well. Therefore, we plan to perform TGA measurements on LIG produced with varying laser powers. These results should confirm or deny our hypothesis about excess laser power melting the neat polymer surrounding LIG regions during LIG formation. Laser PPI can also affect RF response, with lower PPIs corresponding to less RF response. This trend can be attributed to the fact that reducing PPI reduces the amount of LIG (as well as LIG connectivity) produced via laser etching. We also find that LIG connectivity drops below the percolation threshold at 650 PPI.

Our results show that LIG may be used as a heat source to induce polymer diffusion for rapid welding of polymer surfaces. A solid weld may be achieved in just 30 seconds of RF exposure. After performing lap shear testing on welded samples, we find that weld

strength increases with RF exposure time. For rapid welding of polymer surfaces with LIG, weld strength scales with exposure time to the 0.244 power.

Preliminary results also suggest that LIG may be printed and retain RF field responsiveness post-print. After optimizing the print parameters for PEI and PESU filament, we will be able to evaluate the feasibility of using LIG as a nanofiller in 3D printing applications.

REFERENCES

(1) Sweeney, C. B.; Lackey, B. A.; Pospisil, M. J.; Achee, T. C.; Hicks, V. K.; Moran, A. G.; Teipel, B. R.; Saed, M. A.; Green, M. J. Welding of 3D-printed carbon nanotube–polymer composites by locally induced microwave heating. *Science Advances* **2017**, *3*, e1700262.

(2) Sweeney, C. B.; Moran, A. G.; Gruener, J. T.; Strasser, A. M.; Pospisil, M. J.; Saed, M. A.; Green, M. J. Radio frequency heating of carbon nanotube composite materials. *ACS Applied Materials & Interfaces* **2018**, *10*, 27252-27259.

(3) Davenas, J. Laser and ion beam processing of conductive polyimide. *Applied Surface Science* **1989**, *36*, 539-544.

(4) Brom, H.; Tomkiewicz, Y.; Aviram, A.; Broers, A.; Sunners, B. On a new conducting polymer-pyrolyzed Kapton. *Solid State Communications* **1980**, *35*, 135-139.

(5) Srinivasan, R.; Hall, R.; Wilson, W.; Loehle, W.; Allbee, D. Ultraviolet laser irradiation of the polyimide, PMDA-ODA (Kapton™), to yield a patternable, porous, electrically conducting carbon network. *Synthetic Metals* **1994**, *66*, 301-307.

(6) Srinivasan, R.; Hall, R.; Loehle, W.; Wilson, W.; Allbee, D. Chemical transformations of the polyimide Kapton brought about by ultraviolet laser radiation. *Journal of Applied Physics* **1995**, *78*, 4881-4887.

(7) Raimondi, F.; Abolhassani, S.; Brütsch, R.; Geiger, F.; Lippert, T.; Wambach, J.; Wei, J.; Wokaun, A. Quantification of polyimide carbonization after laser ablation. *Journal of Applied Physics* **2000**, *88*, 3659-3666.

(8) Schumann, M.; Sauerbrey, R.; Smayling, M. Permanent increase of the electrical conductivity of polymers induced by ultraviolet laser radiation. *Applied Physics Letters* **1991**, *58*, 428-430.

(9) Phillips, H.; Callahan, D.; Sauerbrey, R.; Szabó, G.; Bor, Z. Sub-100 nm lines produced by direct laser ablation in polyimide. *Applied Physics Letters* **1991**, *58*, 2761-2763.

(10) Feurer, T.; Sauerbrey, R.; Smayling, M.; Story, B. Ultraviolet-laser-induced permanent electrical conductivity in polyimide. *Applied Physics A* **1993**, *56*, 275-281.

(11) Lin, J.; Peng, Z.; Liu, Y.; Ruiz-Zepeda, F.; Ye, R.; Samuel, E. L.; Yacaman, M. J.; Yakobson, B. I.; Tour, J. M. Laser-induced porous graphene films from commercial polymers. *Nature Communications* **2014**, *5*, 5714.

(12) Li, L.; Zhang, J.; Peng, Z.; Li, Y.; Gao, C.; Ji, Y.; Ye, R.; Kim, N. D.; Zhong, Q.; Yang, Y. High-performance pseudocapacitive microsupercapacitors from laser-induced graphene. *Advanced Materials* **2016**, *28*, 838-845.

(13) Chyan, Y.; Ye, R.; Li, Y.; Singh, S. P.; Arnusch, C. J.; Tour, J. M. Laser-induced graphene by multiple lasing: toward electronics on cloth, paper, and food. *ACS Nano* **2018**, *12*, 2176-2183.

(14) Dreyfus, R. CN temperatures above laser ablated polyimide. *Applied Physics A* **1992**, *55*, 335-339.

(15) Jud, K.; Kausch, H. H.; Williams, J. G. Fracture-mechanics studies of crack healing and welding of polymers. *Journal of Materials Science* **1981**, *16*, 204-210.

(16) Boiko, Y. M.; Guerin, G.; Marikhin, V. A.; Prud'homme, R. E. Healing of interfaces of amorphous and semi-crystalline poly(ethylene terephthalate) in the vicinity of the glass transition temperature. *Polymer* **2001**, *42*, 8695-8702.

(17) Vogel, J.; Kessler, M. R.; Sundararajan, S.; Grewell, D. Activation energy for diffusion and welding of PLA films. *Polymer Engineering and Science* **2012**, *52*, 1693-1700.

(18) Prager, S.; Tirrell, M. The healing-process at polymer-polymer interfaces. *Journal of Chemical Physics* **1981**, *75*, 5194-5198.

(19) Kline, D. B.; Wool, R. P. Polymer welding relations investigated by a lap shear joint method. *Polymer Engineering and Science* **1988**, *28*, 52-57.

(20) Wool, R. P.; Yuan, B. L.; McGarel, O. J. Welding of polymer interfaces. *Polymer Engineering and Science* **1989**, *29*, 1340-1367.

(21) Ge, T.; Grest, G. S.; Robbins, M. O. Structure and strength at immiscible polymer interfaces. *ACS Macro Letters* **2013**, *2*, 882-886.

(22) Ge, T.; Grest, G. S.; Robbins, M. O. Tensile fracture of welded polymer interfaces: miscibility, entanglements, and crazing. *Macromolecules* **2014**, *47*, 6982-6989.

(23) Ge, T.; Pierce, F.; Perahia, D.; Grest, G. S.; Robbins, M. O. Molecular dynamics simulations of polymer welding: strength from interfacial entanglements. *Physical Review Letters* **2013**, *110*, 098301.

(24) Dodin, M. G. Welding mechanisms of plastics: a review. *The Journal of Adhesion* **1981**, *12*, 99-111.

(25) Boiko, Y. M.; Guérin, G.; Marikhin, V. A.; Prud'homme, R. E. Healing of Interfaces of Amorphous and Semi-crystalline poly (ethylene terephthalate) in the vicinity of the glass transition temperature. *Polymer* **2001**, *42*, 8695-8702.

(26) Vogel, J.; Kessler, M. R.; Sundararajan, S.; Grewell, D. Activation energy for diffusion and welding of PLA films. *Polymer Engineering & Science* **2012**, *52*, 1693-1700.

(27) Prager, S.; Tirrell, M. The healing process at polymer–polymer interfaces. *The Journal of Chemical Physics* **1981**, *75*, 5194-5198.

(28) Prager, S.; Adolf, D.; Tirrell, M. Welding of polymer networks. *The Journal of Chemical Physics* **1986**, *84*, 5152-5154.

(29) Zhang, H.; Fortin, D.; Xia, H.; Zhao, Y. Fast optical healing of crystalline polymers enabled by gold nanoparticles. *Macromolecular Rapid Communications* **2013**, *34*, 1742-1746.

(30) Chowdhury, S.; Chen, Y.; Wang, Y.; Mitra, S. Microwave-induced rapid nanocomposite synthesis using dispersed single-wall carbon nanotubes as the nuclei. *Journal of Materials Science* **2009**, *44*, 1245-1250.

(31) Higginbotham, A. L.; Moloney, P. G.; Waid, M. C.; Duque, J. G.; Kittrell, C.; Schmidt, H. K.; Stephenson, J. J.; Arepalli, S.; Yowell, L. L.; Tour, J. M. Carbon nanotube composite curing through absorption of microwave radiation. *Composites Science and Technology* **2008**, *68*, 3087-3092.

(32) Shim, H. C.; Kwak, Y. K.; Han, C.-S.; Kim, S. Enhancement of adhesion between carbon nanotubes and polymer substrates using microwave irradiation. *Scripta Materialia* **2009**, *61*, 32-35.

(33) Zhang, H.; Zhao, Y. Polymers with dual light-triggered functions of shape memory and healing using gold nanoparticles. *ACS Applied Materials & Interfaces* **2013**, *5*, 13069-13075.

(34) Cao, Z. X.; Wang, R. G.; Hao, L. F.; Jiao, W. C.; Yang, F.; Wang, Q.; Liu, W. B.; Zhang, B. Y.; Lu, X. L.; He, X. D. Interfacial healing of carbon fiber composites in the presence of gold nanoparticles as localized "nano-heaters". *RSC Advances* **2015**, *5*, 5680-5685.

(35) Vázquez, E.; Prato, M. Carbon nanotubes and microwaves: interactions, responses, and applications. *ACS Nano* **2009**, *3*, 3819-3824.

(36) Baughman, R. H.; Zakhidov, A. A.; de Heer, W. A. Carbon nanotubes - the route toward applications. *Science* **2002**, *297*, 787-792.

(37) Rangari, V. K.; Bhuyan, M. S.; Jeelani, S. Microwave processing and characterization of EPON 862/CNT nanocomposites. *Materials Science and Engineering: B* **2010**, *168*, 117-121.

(38) Brunetti, F. G.; Herrero, M. A.; Munoz, J. d. M.; Diaz-Ortiz, A.; Alfonsi, J.; Meneghetti, M.; Prato, M.; Vazquez, E. Microwave-induced multiple functionalization of carbon nanotubes. *Journal of the American Chemical Society* **2008**, *130*, 8094-8100.

(39) Imholt, T. J.; Dyke, C. A.; Hasslacher, B.; Perez, J. M.; Price, D. W.; Roberts, J. A.; Scott, J. B.; Wadhawan, A.; Ye, Z.; Tour, J. M. Nanotubes in microwave

fields: Light emission, intense heat, outgassing, and reconstruction. *Chemistry of Materials* **2003**, *15*, 3969-3970.

(40) Mashal, A.; Sitharaman, B.; Li, X.; Avti, P. K.; Sahakian, A. V.; Booske, J. H.; Hagness, S. C. Toward carbon-nanotube-based theranostic agents for microwave detection and treatment of breast cancer: Enhanced dielectric and heating response of tissue-mimicking materials. *IEEE Transactions and Biomedical Engineering* **2010**, *57*, 1831-1834.

(41) Paton, K. R.; Windle, A. H. Efficient microwave energy absorption by carbon nanotubes. *Carbon* **2008**, *46*, 1935-1941.

(42) Shim, H. C.; Song, J. W.; Kwak, Y. K.; Kim, S.; Han, C.-S. Preferential elimination of metallic single-walled carbon nanotubes using microwave irradiation. *Nanotechnology* **2009**, *20*, 065707.

(43) Zhang, M.; Fang, S. L.; Zakhidov, A. A.; Lee, S. B.; Aliev, A. E.; Williams, C. D.; Atkinson, K. R.; Baughman, R. H. Strong, transparent, multifunctional, carbon nanotube sheets. *Science* **2005**, *309*, 1215-1219.

(44) Ferrari, A. C.; Meyer, J.; Scardaci, V.; Casiraghi, C.; Lazzeri, M.; Mauri, F.; Piscanec, S.; Jiang, D.; Novoselov, K.; Roth, S. Raman spectrum of graphene and graphene layers. *Physical Review Letters* **2006**, *97*, 187401.

(45) Ferrari, A. C.; Robertson, J. Interpretation of Raman spectra of disordered and amorphous carbon. *Physical Review B* **2000**, *61*, 14095.

APPENDIX A

ADDITIONAL RF AND WELDING CHARACTERIZATION

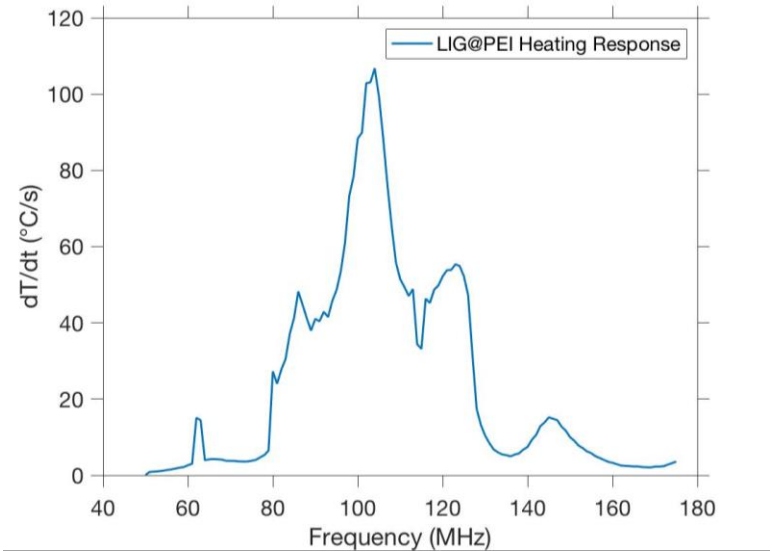

Figure A-1. RF field heating response of LIG@PEI as a function of frequency (Power = 10 W). Table 3-1 lists the laser parameters used to prepare this sample.

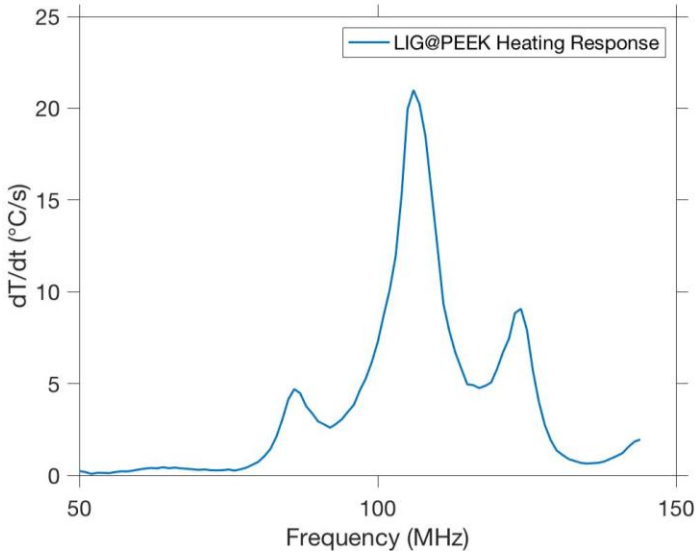

Figure A-2. RF field heating response of LIG@PEEK as a function of frequency (Power = 10 W). Table 3-1 lists the laser parameters used to prepare this sample.

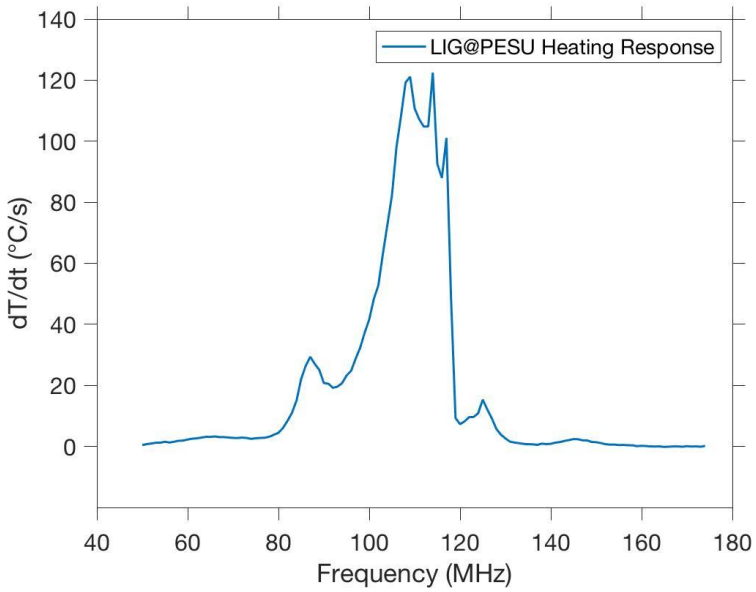

Figure A-3. RF field heating response of LIG@PESU as a function of frequency (Power = 10 W). Table 3-1 lists the laser parameters used to prepare this sample.

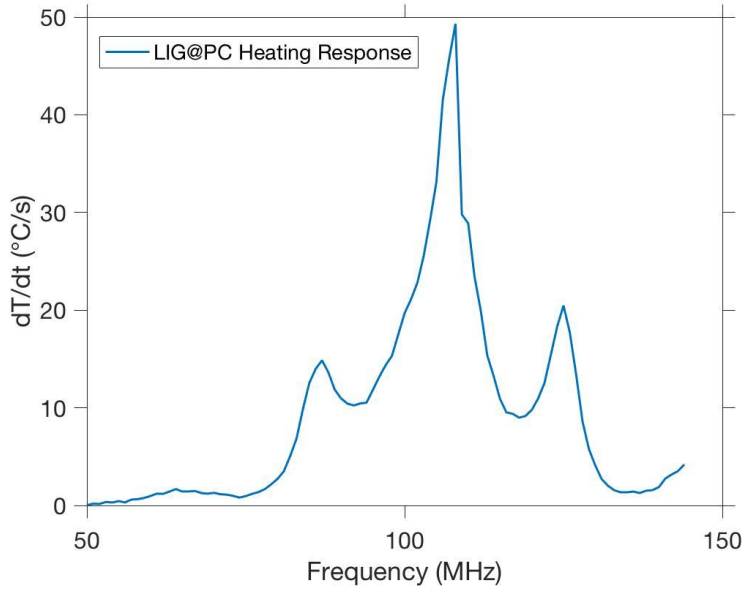

Figure A-4. RF field heating response of LIG@PC as a function of frequency (Power = 10 W). Table 3-1 lists the laser parameters used to prepare this sample.

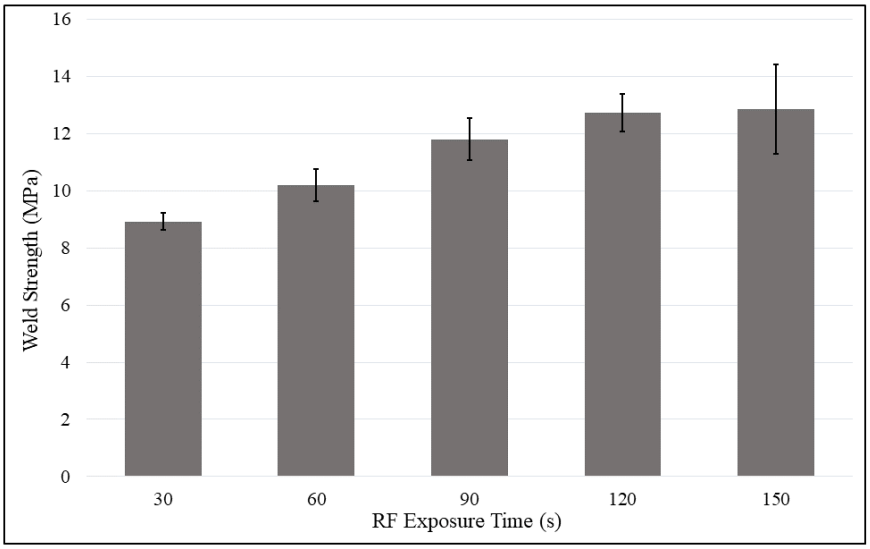

Figure A-5. Graphical representation of the weld strength data presented in Table 3-3. Standard deviation bars for each data set are included.

APPENDIX B

OPTICAL MICROSCOPY AND IMAGES

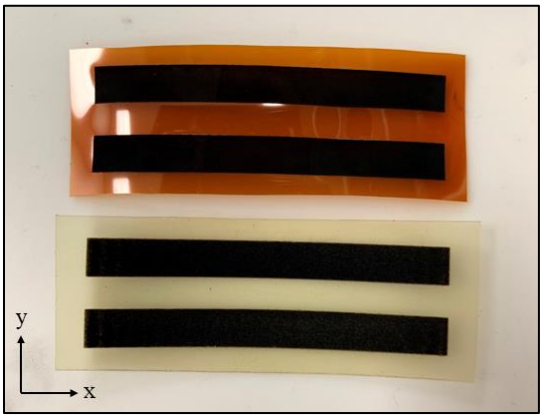

Figure B-1. Image showing the LIG@Kapton (top) and LIG@PEI (bottom) samples that were used for initial RF heating trials and studying the effects of laser power on RF response. Table 3-1 lists the laser parameters used to prepare these samples.

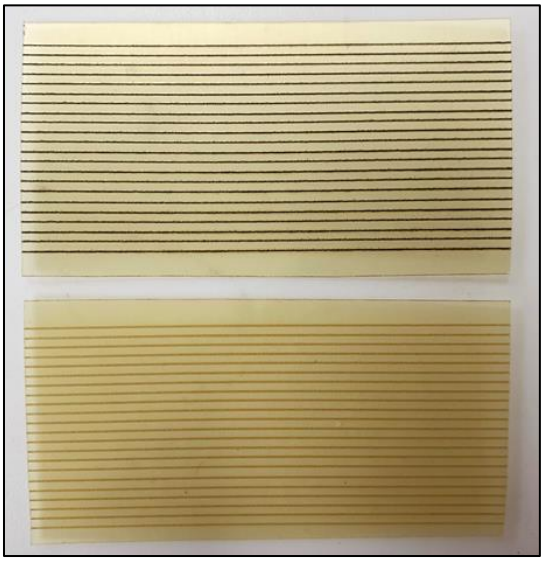

Figure B-2. Image showing LIG@PEI samples that were used for studying the effects of PPI on RF response and LIG morphology. The top sample was produced with 1000 PPI, while the bottom sample with 100 PPI (5% laser power, 10% etch speed).

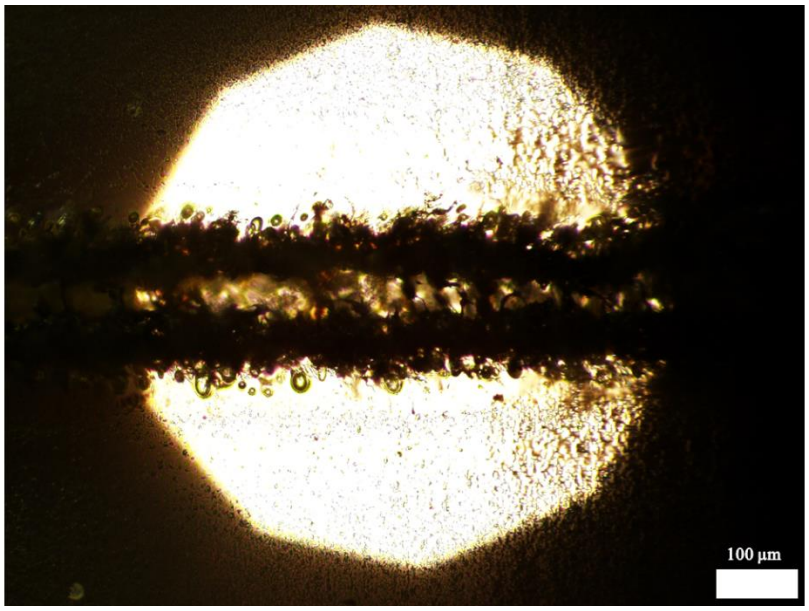

Figure B-3. Optical microscopy image of a single LIG@PEI stripe produced with 1000 PPI (5% laser power, 10% etch speed).

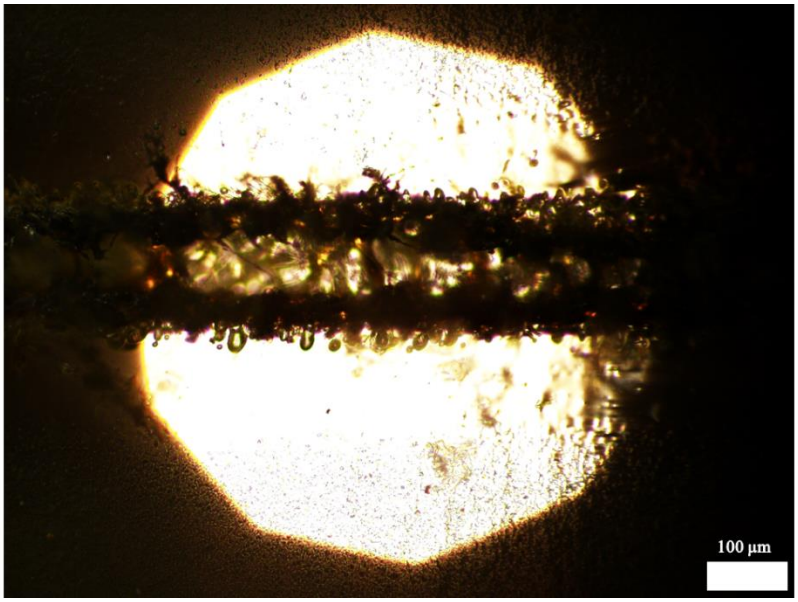

Figure B-4. Optical microscopy image of a single LIG@PEI stripe produced with 700 PPI (5% laser power, 10% etch speed).

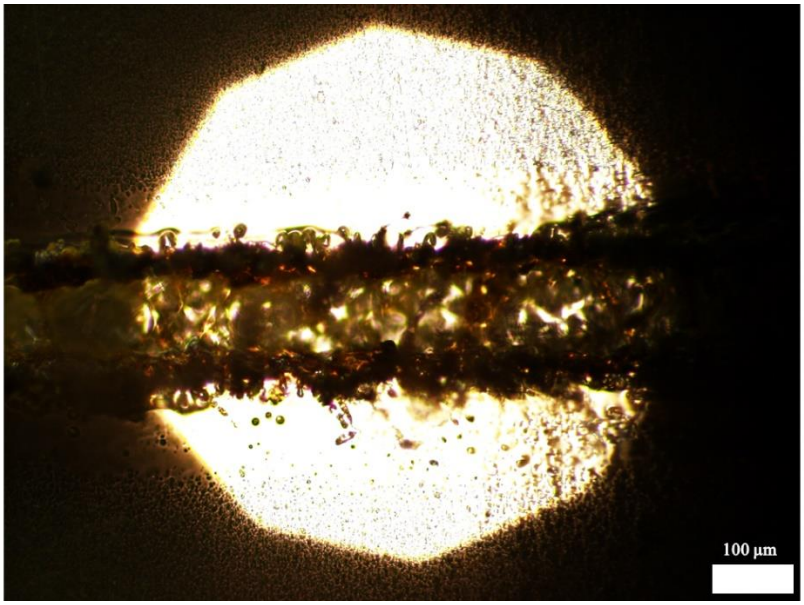

Figure B-5. Optical microscopy image of a single LIG@PEI stripe produced with 650 PPI (5% laser power, 10% etch speed).

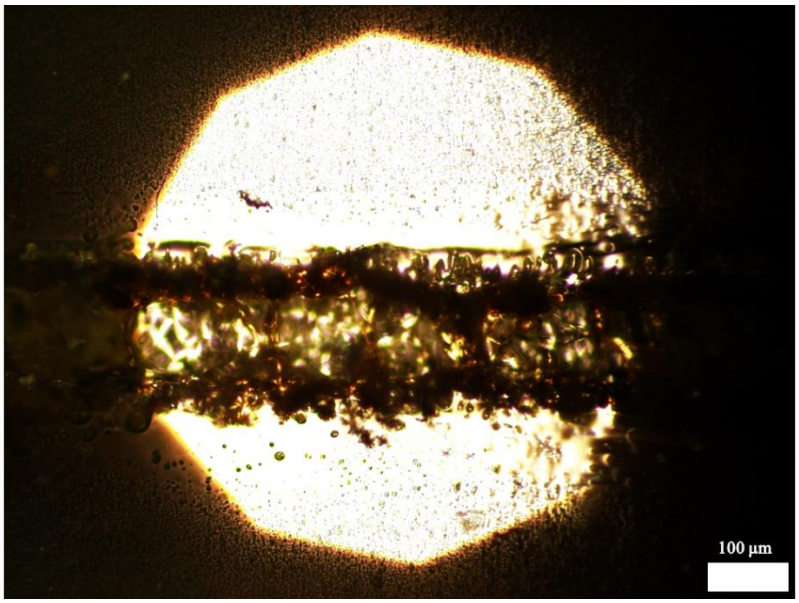

Figure B-6. Optical microscopy image of a single LIG@PEI stripe produced with 625 PPI (5% laser power, 10% etch speed).

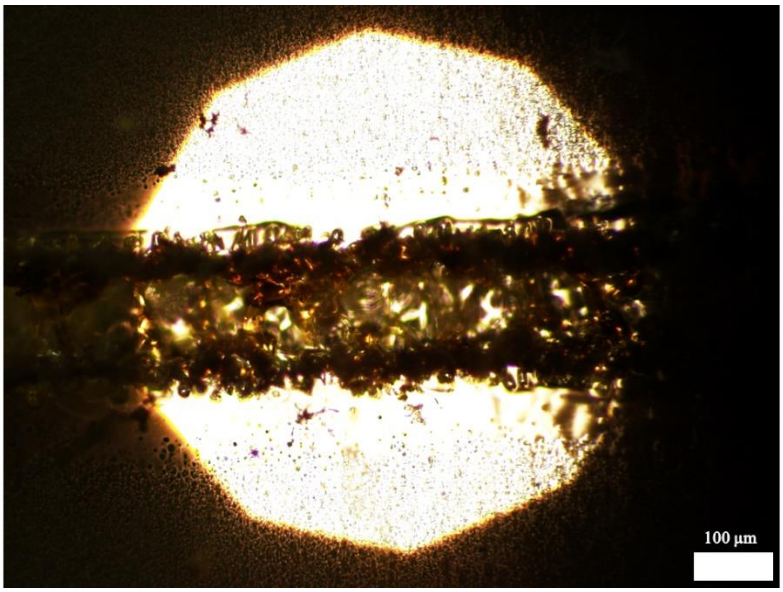

Figure B-7. Optical microscopy image of a single LIG@PEI stripe produced with 600 PPI (5% laser power, 10% etch speed).

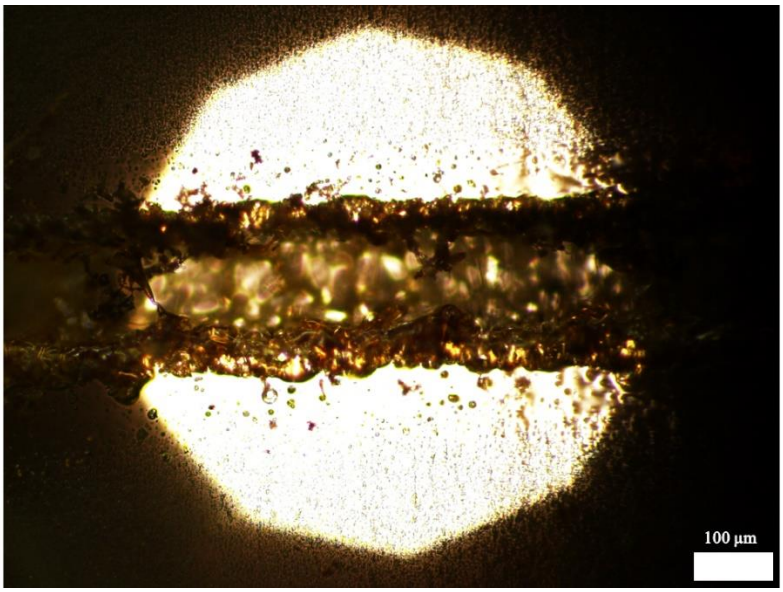

Figure B-8. Optical microscopy image of a single LIG@PEI stripe produced with 300 PPI (5% laser power, 10% etch speed).

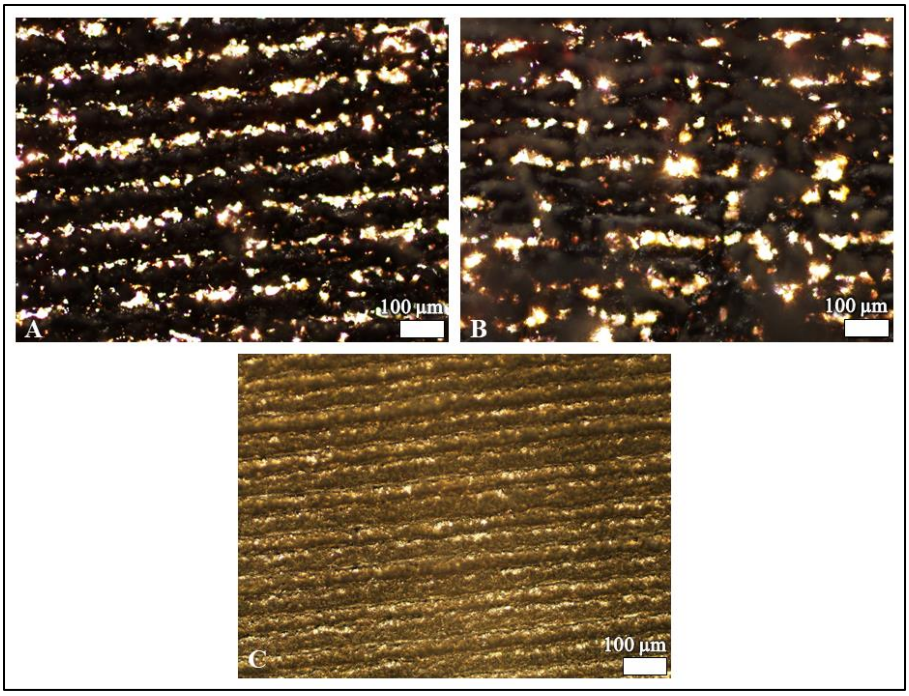

Figure B-9. Optical microscopy images (scale bar=100 µm) of LIG@PEI produced with 5% (A), 7% (B), and 10% (C) laser power (10% etch speed, 1000 PPI).